Universidade de São Paulo–USP
Escola de Engenharia de São Carlos
Departamento de Engenharia Elétrica e de Computação
Programa de Pós-Graduação em Engenharia Elétrica

Daniel Rodrigues de Lima

Analysis of Neurophysiological Signals from the Proprioceptor System of Insects

São Carlos
2016

Daniel Rodrigues de Lima

Analysis of Neurophysiological Signals from the Proprioceptor System of Insects

Dissertação de mestrado apresentada ao Programa de Engenharia Elétrica da Escola de Engenharia de São Carlos da Universidade de São Paulo como parte dos requisitos para a obtenção do título de Mestre em Ciências, Programa de Engenharia Elétrica.

Área de concentração: Sistemas dinâmicos

Supervisor: Prof. Dr. Carlos Dias Maciel

Trata-se da Versão Original
São Carlos
2016

de Lima, Daniel Rodrigues
D184a Analysis of Neurophysiological Signals from the Proprioceptor System of Insects / Daniel Rodrigues de Lima; orientador Carlos Dias Maciel. São Carlos, 2016.

Dissertação (Mestrado) - Programa de Pós-Graduação em Engenharia Elétrica e Área de Concentração em Sistemas Dinâmicos -- Escola de Engenharia de São Carlos da Universidade de São Paulo, 2016.

1. Proprioception. 2. Desert locusts. 3. Sensory neurons. 4. Spiking rates. 5. Delayed transfer entropy. 6. Simulation. I. Título.

FOLHA DE JULGAMENTO

Candidato: Engenheiro **DANIEL RODRIGUES DE LIMA.**

Título da dissertação: "Análise de sinais eletrofisiológicos do sistema proprioceptor de insetos".

Data da defesa: 17/11/2016.

Comissão Julgadora: **Resultado:**

Prof. Associado **Carlos Dias Maciel** APROVADO
(Orientador)
(Escola de Engenharia de São Carlos/EESC)

Prof. Titular **Alberto Cliquet Junior** APROVADO
(Escola de Engenharia de São Carlos/EESC)

Prof. Dr. **Carlos Henrique Costa Ribeiro** APROVADO
(Instituto Tecnológico de Aeronáutica/ITA)

Coordenador do Programa de Pós-Graduação em Engenharia Elétrica:
Prof. Associado **Luís Fernando Costa Alberto**

Presidente da Comissão de Pós-Graduação:
Prof. Associado **Luís Fernando Costa Alberto**

To my family whom I can always count on for love and support.

Acknowledgements

I am grateful to God whose work I try to understand in my studies.

I am thankful to my family for always supporting me and staying with me.

I am also grateful to those friends from the Signal Processing Laboratory that I made in this process.

I am grateful to Professor Carlos Maciel who guided me in this journey.

I would like to express my gratitude to the University of São Paulo, the São Carlos School of Engineering and the Department of Electrical and Computational Engineering for providing me the best academic environment in Latin America. Also, I would like to thank CAPES, the Brazilian Federal Agency for Support and Evaluation of Graduate Education within the Ministry of Education of Brazil.

"Graph models can be used as mathematical language
for integrating statistical and subject-matter information"
PEARL (1995)

Resumo

de Lima, Daniel Rodrigues **Análise de Sinais Eletrofisiológicos do Sistema Proprioceptor de Insetos**. 117 p. Dissertação de mestrado – Escola de Engenharia de São Carlos, Universidade de São Paulo, 2016.

Propriocepção é a capacidade de monitorar a posição do corpo necessária para coordenar movimentos precisos. Apesar da baixa complexidade dos sistemas neuronais de insetos, cientistas têm estudado seu controle motor. Pesquisadores realizaram experimentos em gafanhotos estimulando mecanicamente seu apódema e registrando a resposta neuronal. Estudos anteriores relatam variações nas taxas de *spiking*, e as relacionam com sensibilidades à aceleração, à velocidade e à posição. Seus resultados nos levaram às suposições de que ou existem diferentes tipos de neurônios sensores ou há apenas um tipo de neurônio sensível à diferentes grandezas físicas. Portanto, esta pesquisa pretende investigar as diferentes taxas de *spiking* e estudar a influência das excitações do apódema em neurônios sensores com medidas de teoria da informação. No entanto, a forma como os sinais foram gravados não permite calcular-se a transferência de entropia atrasada (DTE) entre neurônios sensores. Para tanto, propôs-se um método de estimação de parâmetros para ligações em tais cenários. As análises modelarão o tempo gasto entre *spikings* com funções de sobrevida. Além disso, a influência da excitação sobre a resposta neuronal será analisada com DTE, a qual também será utilizada para validar os métodos de simulação. Os resultados mostram que há evidências para suportar a hipótese de diferentes taxas de *spiking*. A DTE sugere a existência de nós intermediários (entre excitação e alguns neurônios sensoriais). Posteriormente, uma simulação juntando os métodos propostos e os sinais neuronais mostrou que modelos considerando caminhos intermediários se ajustam bem aos dados. Por fim, os resultados sugerem que as diferentes respostas de neurônios sensores não acontecem devido a diferentes tipos de neurônios, mas sim à uma camada de pré-processamento.

Palavras-chave: Propriocepção; gafanhotos; neurônios sensores; taxas de *spiking*; transferência de entropia atrasada; simulação..

Abstract

de Lima, Daniel Rodrigues **Analysis of Neurophysiological Signals from the Proprioceptor System of Insects**. 117 p. Master Dissertation – São Carlos School of Engineering, University of São Paulo, 2016.

Proprioception is the ability to sense body position necessary for coordinate precise movements. Despite the low complexity of insect neuronal systems, scientists are studying their motor control system. Researchers performed experiments in desert locusts by stimulating their apodeme and recording the neuronal response. Previous studies reported variations in neuronal spiking rates related to acceleration, velocity and position sensitivity. Their results led us to the assumption that either there are different kinds of sensory neurons, or there is only one type of neuron responding to various Physical quantities. Therefore, this research intends to investigate the different spiking rates. We also want to study the influence of apodeme's excitations in sensory neurons with information theoretical measures. However, the way signals were recorded does not allow the calculation of delayed transfer entropy (DTE) between sensory neurons. To solve that problem we propose a method to estimate parameters of connections in such scenarios. Our analysis will model the time spent between spikes with survival functions. The influence of excitation in the neuronal response will be analyzed with DTE, which will also be used to validate the methods of simulation. Results show that there is evidence to support the assumption of different spiking rates among sensory neurons. DTE suggests the existence of intermediate processing nodes between excitation and some sensory neurons. A further simulation joining the methods proposed and neuronal signals showed that models considering intermediate pathways present a good fit to the data. We suggest that the different responses of sensory neurons are not due to various types of neurons, but to a preprocessing layer.

Keywords: Proprioception; desert locusts; sensory neurons; spiking rates; delayed transfer entropy; simulation..

List of Figures

List of Tables

Contents

Chapter 1

Introduction

Proprioception is the "*notion of self-perception*" (HILLIER; IMMINK; THEWLIS, 2015), the ability by which is possible to have a sense of body position and orientation. Without it, deafferented people require visual information to coordinate their movements (SARLEGNA et al., 2010). However, even with visual feedback, they cannot perform some simple daily tasks, such as handling tools (CARDINALI et al., 2016).

By the proprioceptive process, the body can sense its own movements. For rehabilitation purposes, for example, the knowledge about proprioception is important to properly plan and apply treatments (CUPPONE et al., 2015). Several devices are being developed in order to assist the recovery of proprioceptive functions. Examples include the ankle-foot system *PNF - Proprioceptive Neuromuscular Facilitation* (ZHOU et al., 2015) and robot-assisted therapies (HUGHES et al., 2015; COLOMBO et al., 2016)

As Reinstein and Hoffmann (2013) said, proprioception "*is a strong requirement for any mobile agent, animal or robot, to be able to estimate its posture and to gauge the distance it travelled*". Thus, nowadays scientists are directing their attention to animals proprioceptive systems (REINSTEIN; HOFFMANN, 2013). Such approach of investigating nature's answer to engineering related problems constitutes the biologically inspired engineering (ZHANG et al., 2015).

The scientific community is studying Arthropods' physiology, since their leg control system presents similarities to mammals' (BUSCHMANN et al., 2015). Although the arthropods nervous system is a relatively simple structure (compared to mammals), its behavior is equivalent to more complex structures (VIDAL-GADEA et al., 2010). In a particular case, desert locusts (insects) present a distributed nervous system, which is of great interest due to its capability of "*integrate behaviors, perform pattern recognition, context-dependent learning, and combine many sensory inputs*" (WESSNITZER; WEBB, 2006).

In desert locusts, the organ responsible for the hind leg motor control is the metathoracic ganglion (DEWHIRST, 2012). With only 2000 neurons this organ receives input signals from the insect hind leg, process the information received and acts controlling leg movements (BURROWS, 1996). The *Femorotibial Chordotonal Organ (FeCO)* in the

locust hind leg, together with its *sensory neurons (SN)*, converts movements from the locust hind leg into neuronal spiking signals (KONDOH; OKUMA; NEWLAND, 1995).

A previous study (KONDOH; OKUMA; NEWLAND, 1995) reported the existence of different spiking rates among those signals. It also reported that some neurons would respond to acceleration, while others would be sensible to position, and some would to velocity (KONDOH; OKUMA; NEWLAND, 1995). They pointed that signals with low spiking rates should be records of neurons sensitive to acceleration. In the opposite side, high spiking rates would be related to position sensitivity, and the velocity sensitive neurons would present an intermediate spiking rate. Here in this study, our first goal is to test the hypothesis of different spiking rates among sensory neuron signals. Additionally, we want to know if it is possible to group signals with similar characteristics. To do so, we will model the time interval spent between spikes, the *inter-spiking-interval (ISI)*, with survival functions (ACHCAR; MOALA, 2015).

In the experiments made by Kondoh, Okuma and Newland (1995), they simulated leg movements by applying mechanical excitations in the insect apodeme and recorded the neuronal response. In their studies, methods of system identification were applied in signals from individual neurons, with approaches varying from black-box techniques (MERUELO et al., 2016; DEWHIRST et al., 2013) to directed information measures (ENDO et al., 2015; MACIEL; SIMPSON; NEWLAND, 2012). The latter investigated the internal structure of neuronal pathways with time-delayed mutual information (DMI) (SORIANO et al., 2012).

With time sweepings in the calculation of mutual information (COVER; THOMAS, 2006), DMI finds the point of synchronization between two time series. In this study, we adopted a similar technique, the time-delayed transfer entropy (DTE) (SCHREIBER, 2000). It can be represented in terms of mutual information (WIBRAL; VICENTE; LINDNER, 2014), yet being able to distinguish between exchanges and simple shares of information (SCHREIBER, 2000) (see Subsection 3.2.1 for further details). Our second goal here is to apply DTE in the locust data to test the influence of excitation signals in the neuronal response. Additionally, we want to understand if among recorded experiments the ways that excitation influences sensory neurons are the same.

The time-delayed measures of connectivity presented require signals simultaneously recorded, otherwise, results are not guaranteed to reflect the reality. However, due to experimental limitations (the number of simultaneous channels available in record systems is limited (RITZMANN; BÜSCHGES, 2007)) it was not possible to simultaneously record signals from all the nodes of the system. For example, in Endo et al. (2015) study it was only possible to record data from four channels. Such limitation disallows to calculate DTE between sensory neuron signals. Studies argue that simulations can help in such scenarios with experimental constraints (BUSCHMANN et al., 2015). Therefore, the third goal is to develop a method for estimating parameters of interaction between nodes (joint

probability distributions) in such scenarios.

Objectives

The main objective of this dissertation is to study the process of proprioception in the desert locust, by analyzing data from experiments previously developed (KONDOH; OKUMA; NEWLAND, 1995). Our objectives are threefold: analyze neuronal signals investigating the existence of different spiking rates; study with DTE the influence of hind leg stimulus in the neuronal response; develop a method to estimate parameters of connections indirectly.

We want to model the insect proprioceptor system by analyzing neurophysiological recordings, using information theoretical measures and an algorithm for parameter estimation. Specifically, our objectives are:

- ❏ Implement a method for indirectly estimate parameters;
- ❏ Test and validate our algorithms with DTE;
- ❏ Analyze sensory signals modeling the time spent between spikes;
- ❏ Identify different spiking rates;
- ❏ Build models to represent the spiking rates;
- ❏ Apply DTE in controlled signals to test DTE calculation;
- ❏ Apply DTE between excitation and neuronal signals;
- ❏ Apply our methods of simulation in the locust data.

Text Organization

Chapter 2 presents biological concepts regarding desert locusts, such as its nervous system and the hind leg neurons. In the same chapter, we also introduce the locust experiment. Chapter 3 brings concepts from information theory. It presents mutual information and some of its properties (COVER; THOMAS, 2006) relevant to the discussion of our results. Additionally, it presents the measure of DTE and algorithms for generating surrogate time series.

The first part of Chapter 4 presents the methodology used in our analysis. The second part reviews the methods for generating synthetic data following probability distributions and provides an extension for graph-based models. In the third part, we introduce the method proposed for indirectly estimating parameters of interaction.

The first section of Chapter 5 presents the validation of our methods with DTE. The second section presents the analysis of spiking rates and models for the time intervals

between spikes. The third section presents DTE measures analyzing the influence of the excitation in the neuronal response. The fourth section joins the methods of simulation and previous analysis to show that it is reasonable to consider shares of information between sensory neurons. In the last chapter, we present the discussion and conclusions of our results. In addition, we attached the manufacturer's specification notes to the end of this text for documentation purposes.

Chapter 2

Desert Locust

Desert locusts, *Schistocerca gregaria* (Forskål), are animals from the Arthropoda phylum that put their eggs in sandy soils and are usually found in deserts of Africa and Asia. They are a type of grasshoppers, insects with long back legs that can jump very high and make sounds with their legs. Desert locusts feed themselves on leaves, flowers, fruits, seeds, stems, and barks. Locusts swarms require attention since they can damage entire plantations by consuming, in one day, the same amount of food as thousands of people. For this reason, sometimes they are associated with plagues and food crisis, such as the 2004 Africa plague[1].

These animals present a distributed nervous system (see Figure 1), where each ganglion is responsible for the control of one body function. Thoracic ganglia are responsible for the motor control, and the metathoracic ganglion controls the movements of the hind leg. Previous studies (KONDOH; OKUMA; NEWLAND, 1995) recorded signals from a proprioceptor organ and these signals are analyzed in this study. We present the next two sections with a description of the locust neurophysiology and the experiment that recorded signals from sensory neurons.

2.1 Neuronal Sensoring in Locusts Hind Leg

Differently from other animals, insects present a distributed nervous system, i.e., Their neuronal structure is not centralized in the brain. Each part of the body is locally controlled by a specific region of its nerve cord (ganglions) near to it, Figures 1 and 2.

The nervous system of these insects can be divided into two parts: the brain, and the ventral nerve cord. The brain determines insect behavior and sets the direction and the speed of its movements. The ventral nerve cord contains ganglions that locally controls

[1] "Locust plague threatens Africa"; Nature News; [Online] Published on 9 July 2004 at `http://www.nature.com/news/2004/040709/full/news040705-8.html;doi:10.1038/news040705-8`; Accessed in 31 May 2016.

Figure 1: Representation of a desert locust, *Schistocerca gregaria (Forskål)*, highlighting its hind leg and nervous system (nerve cord) segmented in three parts: the brain (green), the thoracic ganglia (orange), and the abdominal ganglia (blue). The thoracic ganglia studied here is responsible for the insect motor control.

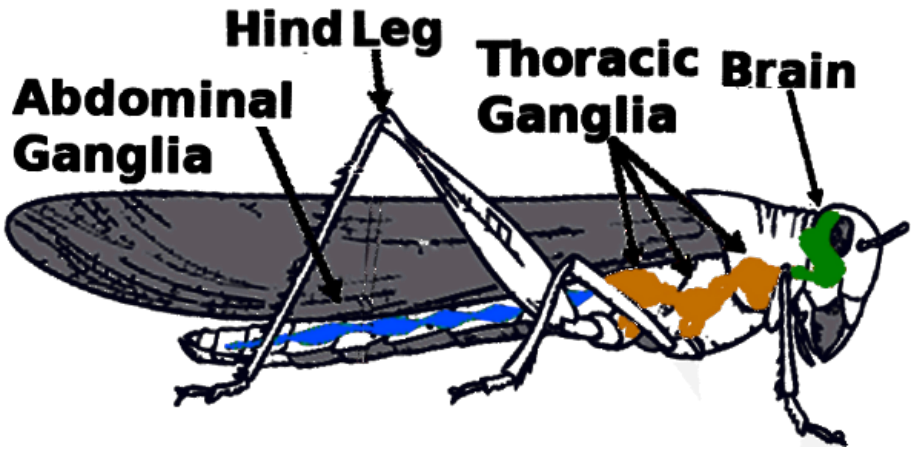

Source: Adapted from Dewhirst (2012).

parts of the body, and can be divided into two parts: the thoracic ganglia, and the abdominal ganglia.

Figure 2: Representation of a desert locust and its distributed nervous system, highlighting at the top its metathoracic ganglion responsible for the local control of the hind leg. The ganglions that compose the locust nervous system are presented following the color scheme of Figure 1.

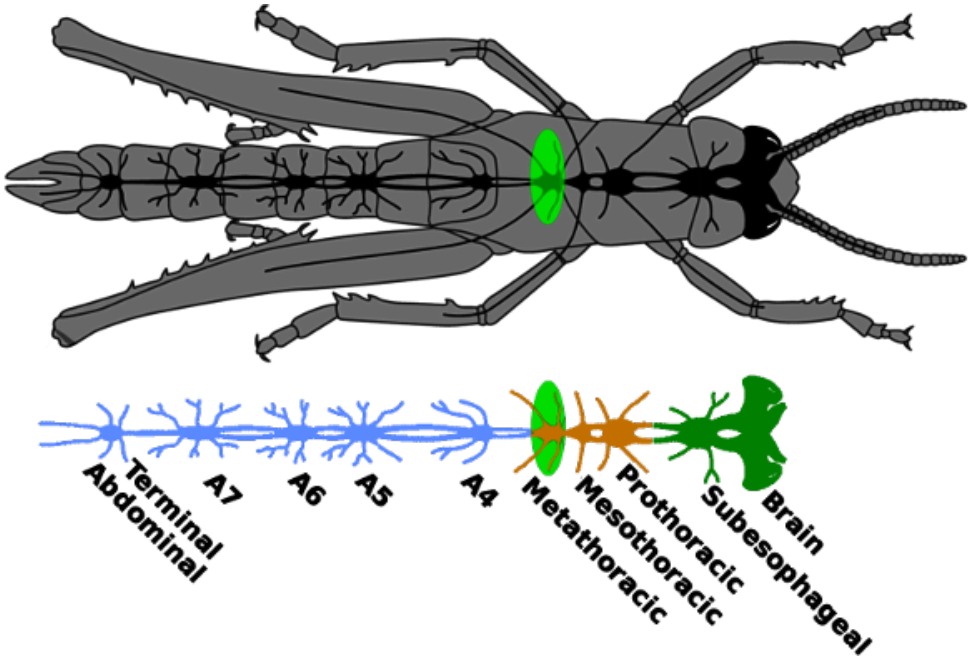

Source: Adapted from Pflüger and Duch (2011).

Abdominal ganglia are responsible for the control of insect body functions, and thoracic ganglia for its motor control (BHARADWAJ; BANERJEE, 1971). Sensory neurons in the insect's leg detect its positions and convert them into neuronal signals. These signals are sent to the thoracic ganglia, where they are processed, and translated into the information used for the motor control (BURROWS, 1996).

A distributed control system is a concept of interest for bio-inspired Engineering (BAR-COHEN, 2006). It is expected that its understanding would lead to simplifications in control architectures. Examples of possible applications include robotics, automation, and the development of prostheses (WESSNITZER; WEBB, 2006).

Three ganglions compose the thoracic ganglia, and each one of them is responsible for the control of one pair of legs (see Figure 2). These three are the prothoracic ganglion, the mesothoracic ganglion, and the metathoracic ganglion. The focus of this study is the metathoracic ganglion, which acts controlling the insect hind legs (DEWHIRST et al., 2009).

The metathoracic ganglion controls and process signals originated by movements of locust hind legs. It is bilaterally symmetric and composed by approximately 2000 neurons. This is a small yet sufficient number of neurons to control, monitor, and process the information from the insect hind legs. Figure 3 presents the metathoracic ganglion in details with its internal structure and types of neurons, and Table 1 present the name of each one of those (see Burrows (1996) for more information).

2.1.1 Sensory Neurons

In the insect femorotibial joint, there is a muscular ligament named apodeme (see Figure 4). Movements of the femorotibial junction in one direction stretch the apodeme, while joint movements in another direction relax it, evoking different responses from sensory neurons.

FeCO is an elastic fiber with approximately 90 sensory neurons that codify information from the apodeme. It helps to convert movements from the locust hind leg into neuronal signals and also transmits them to motor neurons. This transmission is done either directly or indirectly, i.e., from sensory neurons to motor neurons, or passing by interneurons in the metathoracic ganglion.

The hind leg proprioception is done by FeCO and sensory neurons that codify leg angles and emits spike signals. Previous studies analyzed its response intending to understand the proprioception process (KONDOH; OKUMA; NEWLAND, 1995). They excited the neuronal system by shaking the insect leg and recorded the neuronal response.

In such experiments, they found different neuronal responses. The difference appeared either when varying the excitation, or when comparing the spike rates of experiments with the same excitation. As Figure 5 shows, we can visually identify that the spike rates of these two samples are different (they are presented in same the time window of 10 ms).

Figure 3: The metathoracic ganglion responsible for the local motor control of locust's hind leg, and its internal components represented with a 100μm scale (see Table 1 and Burrows (1996) for more information).

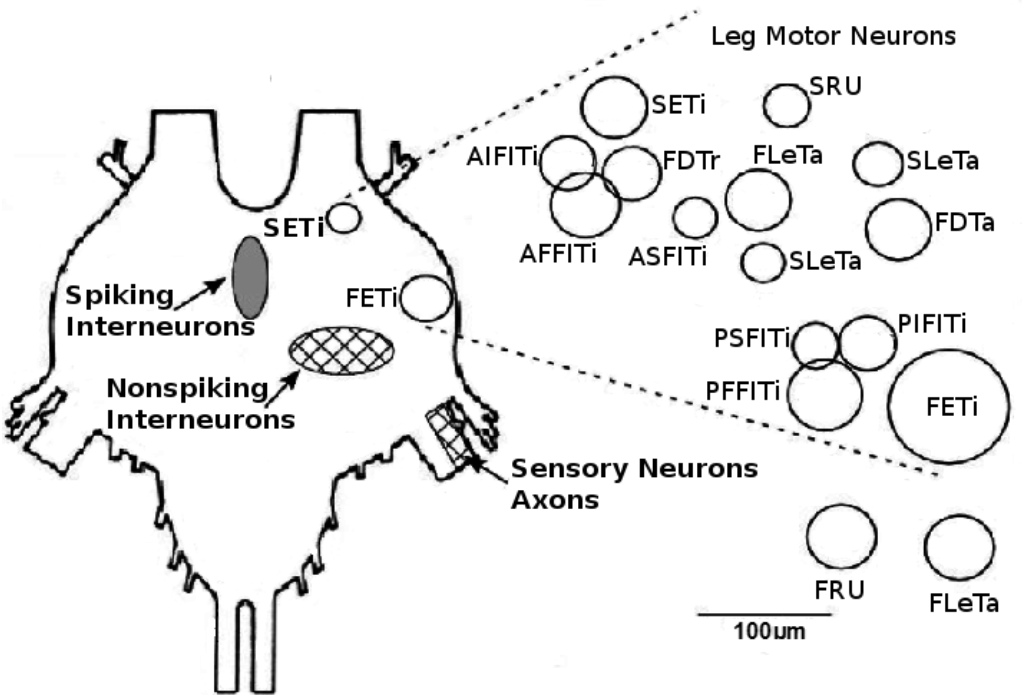

Source: Adapted from Burrows (1996).

The different spiking rates were linked to sensibilities of sensory neurons, such as sensibility to position, velocity or acceleration. However, our goal is to investigate the different spiking rates and divide experiments into groups with similar responses.

2.2 The Neuronal Experiment

Previous studies (KONDOH; OKUMA; NEWLAND, 1995) analyzed sensory neurons responses when FeCO was excited by a Gaussian white noise (GWN). They identified two groups with different spiking rates, and the variety of FeCO responses were related to specific proprioception functions.

At that time, their interest was in the relationship between input and output signals (a black box approach). We will employ a statistical analysis and information theoretical measures to infer about internal connections and information exchanges among sensory neurons.

Data Collection

Adult desert locusts, male and female, were arranged ventral-side-uppermost in modeling clay at room temperature (21.5±°C, relative humidity 35.7±3.7%) (DEWHIRST et al.,

Table 1: Name of each neuron inside the metathoracic ganglion shown in Figure 3.

Femorotibial Joint Movements	
ASFlTi	Anterior Slow Flexor tibia motor neurone
AFFlTi	Anterior Fast Flexor tibia motor neurone
AIFlTi	Anterior Intermediate Flexor tibia motor neurone
PSFlTi	Posterior Slow Flexor tibia motor neurone
PFFlTi	Posterior Fast Flexor tibia motor neurone
PIFlTi	Posterior Intermediate Flexor tibia motor neurone
SETi	Slow Extensor Tibia motor neurone
FETi	Fast Extensor Tibia motor neurone
Tarsus Movements	
SleTa	Slow Levator Tarsus
FleTa	Fast Levator Tarsus
SDTa	Slow Depressor Tarsus
FDTa	Fast Depressor Tarsus
Retractor Unguis Movements	
SRU	Slow Retractor unguis motor neurone
FRU	Fast Retractor unguis motor neurone
Trochanter Joint Movements	
FLeTr	Fast Levator Trochanter motor neurone
FDTr	Fast Depressor Trochanter motor neurone

2011). In their anterior distal femur, a piece of cuticle was cut to expose FeCO apodeme (KONDOH; OKUMA; NEWLAND, 1995). FeCO was gripped by a forceps that was attached to a shaker (Ling Altec 101).

A small window in the ventral thorax exposed the metathoracic ganglion. Before start recording, the sheath was treated with protease (Sigma type XIV) for 1 minute. Then, potassium acetate microelectrodes, with DC resistances of 50-80 MΩ, were driven through the sheath. An Axoclamp 2A amplifier[2] (Axon Instruments, USA) was used for intracellular recordings.

A GWN band-limited to 200 Hz was produced by a pseudo random binary sequence (CG-742, NF Circuit Design Block[3]). A low-pass filter with a decay of 24 dB/octave (SR-4BL, NF Circuit Design Block[4]) was used to produce GWN band-limited to 27 Hz or 58 Hz from the original 200 Hz signal. Thus, generating a Gaussian white noise in the bandwidth of interest.

[2]Axoclamp 2A amplifier [online] accessed on 03 June 2016, available at: `https://www.moleculardevices.com/systems/conventional-patch-clamp/axoclamp-900a-microelectrode-amplifier`.

[3]CG-742, NF Circuit Design Block [online] accessed on 03 June 2016, available at: `http://www.nfcorp.co.jp/english/pro/fm/osc/index.html`.

[4]SR-4BL, NF Circuit Design Block [online] accessed on 03 June 2016, available at: `http://www.nfcorp.co.jp/english/pro/fm/fil/res/sr/index.html` .

Figure 4: The Femorotibial Chordotonal Organ (FeCO) location in the desert locust hind leg. Insect movements stretch or relax the apodeme, and they are converted to neuronal signals by the FeCO.

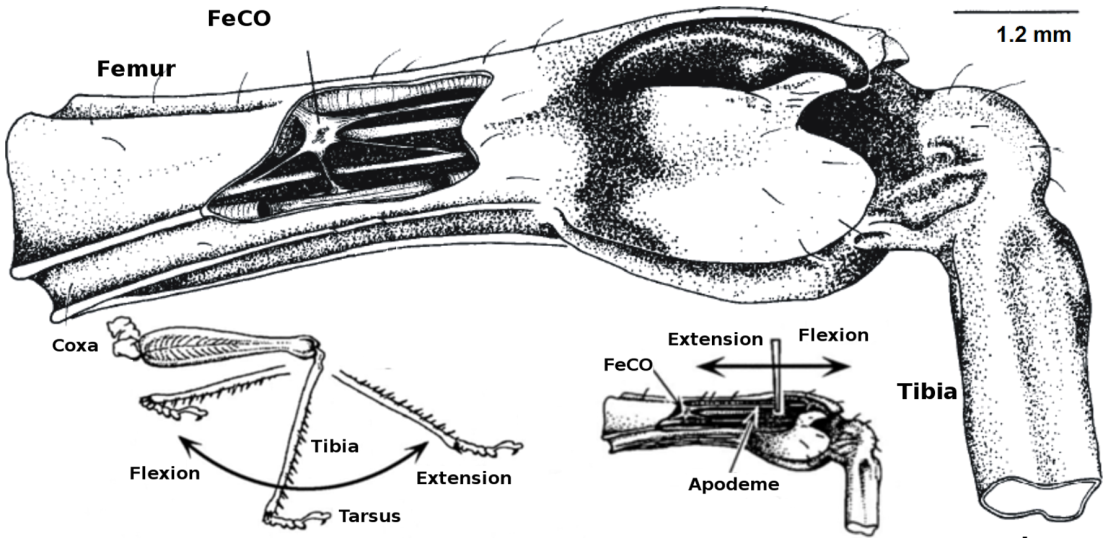

Source: Adapted from Burrows (1987).

Figure 5: Samples of two different spiking rates for the same excitation, suggesting the existence of different neuronal responses. Signals in a time window of 10 ms.

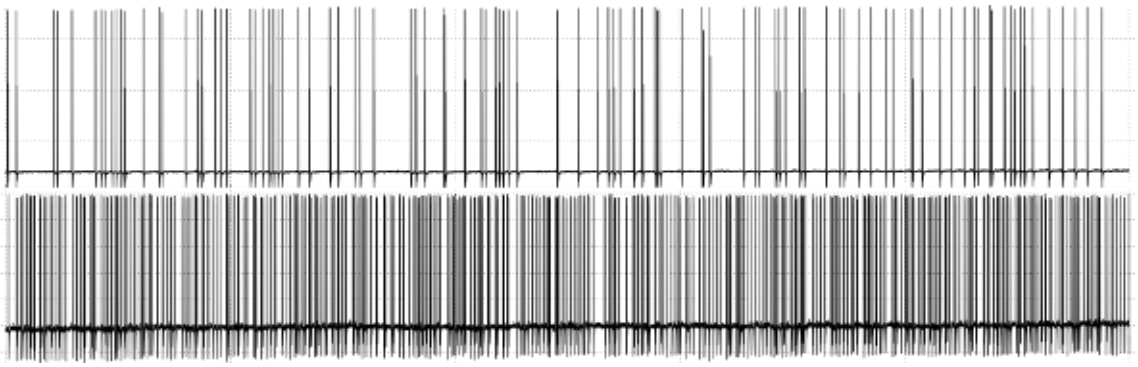

Source: Generated by the author.

Filtered GWN shook the forceps holding the apodeme. Potassium microelectrodes entered into the neuropil processes of the non-spiking local interneurons, the axons of sensory neurons. The band-limited GWN vibrated the forceps evoking neuronal responses. Their signals were collected and stored on magnetic tape using a PCM-DAT data recorder (RD-101 T, TEAC, Japan[5], see Attachment D for further details).

Further, all signals were sampled to a computer for further offline analysis. A representation of the experimental data recorded is shown in Figure 6 with the 200 Hz GWN, the 27Hz GWN, and the sensory neuron response. Also, a representation of the experiment with leg movements, and its simulation is presented in the same figure. Finally, the

[5]RD-101 T, TEAC, Japan [online] accessed on 03 June 2016, available at: `http://www.atecorp.com/products/teac/rd-101t.aspx`.

analyzed signals and a data set description are presented in next section.

Figure 6: Simulation of the locust hind leg movements with apodeme's flexion and extension to excite the nervous system, evoking spiking responses (left). GWN signal band-limited to 200 Hz (right top); filtered GWN signal, 27 Hz (right middle), and sensory neurons spiking response (right bottom).

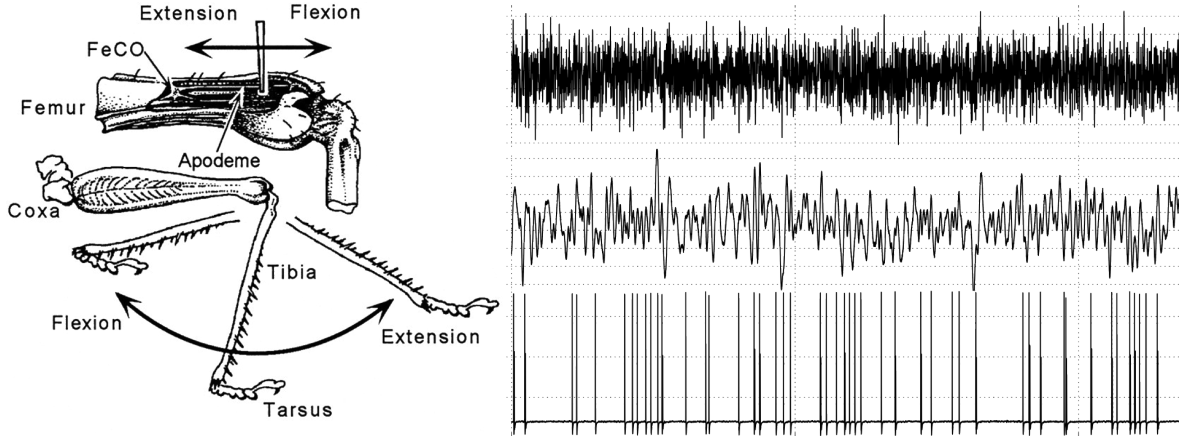

Source: Adapted from Newland and Kondoh (1997).

Analyzed Signals

Excitation signals, GWN band-limited to 27 Hz or 58 Hz shook a forceps attached to the insect apodeme. This stimulation evoked sensory neurons responses producing spiking signals. From the data set, we chose the 39 experiments presented in Table 2. Data is organized as follows: the experiment ID; the bandwidth of excitation signal; the frequency of sample; the four channels with data recorded; and the animal number.

When a channel presents a character X, it means that the signal in that entry is not part of the experiment, and it is not considered. Some experiments present excitation signals with the entry 58/27, and this means that one-half of the experiment was made with one frequency, and the other half with another frequency. In these cases, we divided the experiments into two samples before starting the analysis.

Table 2: Analyzed experiments in the data set.

Experiment ID	Excitation (Hz)	Sampling Frequency (kHz)	Channel 0	1	2	3	Animal Number
ID-701	27	24	X	SN	27	200	18
ID-702	27	24	X	SN	27	200	18
ID-765	58	24	X	SN	27	200	22
ID-766	58/27	24	X	SN	27	200	22
ID-767	58	24	X	SN	27	200	22
ID-773	27	24	X	SN	27	200	22
ID-774	27	24	X	SN	27	200	22
ID-778	27	24	X	SN	27	200	22
ID-780	58	24	X	SN	27	200	22
ID-781	27	24	X	SN	27	200	22
ID-923	27	10	SN	X	27	200	25
ID-924	58	10	SN	X	58	200	25
ID-926	27	10	SN	X	27	200	25
ID-927	58	10	SN	X	58	200	25
ID-929	27	10	SN	X	27	200	25
ID-930	58	10	SN	X	58	200	25
ID-932	27	10	SN	X	27	200	25
ID-934	27	10	SN	X	27	200	25
ID-935	58	10	SN	X	58	200	25
ID-937	27	10	SN	X	27	200	25
ID-945	27	10	SN	X	27	200	25
ID-946	58	10	SN	X	58	200	25
ID-948	27	10	SN	X	27	200	25
ID-1004	27	24	SN	X	27	200	26
ID-1005	58	24	SN	X	58	200	26
ID-1006	27	24	SN	X	27	200	26
ID-1008	27	24	SN	X	27	200	26
ID-1009	58	24	SN	X	58	200	26
ID-1010	27	24	SN	X	27	200	26
ID-1011	58	24	SN	X	58	200	26
ID-1013	27	24	SN	X	27	200	26
ID-1014	58	24	SN	X	58	200	26
ID-1016	27	24	SN	X	27	200	26
ID-1017	58	24	SN	X	58	200	26
ID-1019	27	24	SN	X	27	200	26
ID-1020	58	24	SN	X	58	200	26

Chapter 3

Information Theoretic Concepts

Information Theory was created in the early 1940s, a time when electrical engineers believed to be impossible to transmit messages without losses. That idea was changed when two concepts were introduced by Shannon (COVER; THOMAS, 2006): *Shannon's entropy* and the *channel capacity*.

Shannon proved that for messages bellow the channel capacity the probability of error in transmission could be near to zero (MCDONNELL; IKEDA; MANTON, 2011). He also argued that random processes have an irreducible complexity. He gave the name *entropy* to this complexity, in deference to the entropy found in the thermodynamics field (COVER; THOMAS, 2006).

At a macroscopic level, entropy is the internal energy of a substance that is not accessible to produce work. For the statistical mechanics, entropy is the portion of a system's internal energy that is randomly distributed as kinetic energy (DINCER; CENGEL, 2001). In the thermodynamics field, Boltzmann provided the connection between these two conceptions of entropy. He associated the macroscopic concept of entropy with the logarithm of the number of microstates within a system (LINDLEY, 2001 apud COVER; THOMAS, 2006).

Entropy can be generically defined as "a way of measuring the lack of order that exists in a system"[1]. Then, by measuring the portion of a system's internal energy that is unavailable to produce work, it can represent the disorder of such system.

Entropy is described as a representation of disorder, and also as a measure of a 'disordered' energy (DINCER; CENGEL, 2001). In the same way, Shannon's entropy is defined by Cover and Thomas (2006) as a measure of *uncertainty*. Since it is calculated over probability distributions and not energy, it refers to unpredictability. Therefore, the higher the entropy of a system, the higher the uncertainty in the determination of its states.

The development of information theoretical entropy[2] was one of the initial steps into

[1] Sample of the definition of *entropy* provided by the dictionary "Oxford Learner's Dictionaries"; [Online] accessed on 07 June 2016, available at: `http://www.oxfordlearnersdictionaries.com/definition/english/entropy?q=entropy`.

[2] Since this point, we will only say entropy, H or $H(X)$ when referring to Shannon's entropy.

the field of Information Theory. Later, Kullback and Leibler introduced the concept of relative entropy (KULLBACK; LEIBLER, 1951 apud COVER; THOMAS, 2006), which has been widely applied in the areas of machine learning and pattern recognition (RAJANNA; CAO; VISWANATHAN, 2016; YU et al., 2013; GOLDBERGER; GORDON; GREENSPAN, 2003).

Relative entropy became known either as *Kullback- Leibler divergence* or just *KL-divergence*. It forms the base for Mutual Information (MI), which by its turn is a basic concept for association measures. MI was first introduced by Shannon and measures the amount of information shared by two random variables (MCDONNELL; IKEDA; MANTON, 2011). Based on probability distributions, it can determine if two random variables are independent of each other (COVER; THOMAS, 2006).

From the concept of mutual information, studies developed the method named time-delayed mutual information (JIN; LIN; HALLETT, 2010), or just delayed mutual information (DMI). This measure is capable of investigating associations between process with different time-lags, thus finding interaction time delays.

Schreiber (2000) presented the concept of Transfer Entropy, which is also based on mutual information. He showed that mutual information is not capable of distinguishing between information shared and exchanged. Thus, its results cannot guarantee a cause-effect relation, while transfer entropy does. Further, Wibral et al. (2013) showed that it would also be possible to use transfer entropy to investigate time-delays.

This Chapter is organized first by presenting basic concepts of Information Theory, such as entropy and mutual information in the next sections. The following section presents the definition of Transfer Entropy, and the last one introduces the concept of Surrogate Time Series.

3.1 Entropy and Mutual Information

Cover and Thomas (2006) present entropy as a measure of a random variable's uncertainty. The entropy H of a discrete random variable X, with alphabet $\mathcal{X}$, and probability mas function $p(x) = Pr\{X = x\}, x \in \mathcal{X}$ is defined to be calculated by the following expression

$$H(X) = -\sum_{x \in \mathcal{X}} p(x)\ log\ p(x). \tag{1}$$

If the logarithm is calculated with base e, i.e., $ln\ p(x)$, $H(X)$ is measured in units of *nats*. If the base[3] of the *log* in entropy's equation is 2, i.e., $H(X) = p(x)log_2 p(x)$, the units of entropy are given in *bits* (COVER; THOMAS, 2006).

[3]In this research, we will only use logarithms with base 2 along with information theoretical measures, i.e., $H(X) = -\sum_{x \in \mathcal{X}} p(x)\ log_2\ p(x)$.

A deterministic system presents a well-known response due to an input, and such response does not present variations. The probability distribution of the states in such system is given by

$$\begin{cases} p(X = x_i) = 0, & i = 1, 2, \cdots, n-1 \\ p(X = x_i) = 1, & i = n, \end{cases} \tag{2}$$

where n stands for the number of possible states. In such case, the unpredictability of the system is the minimum possible, and its entropy is zero as a consequence of the convention

$$\lim_{t \to 0} \; t \cdot log(t) = 0. \tag{3}$$

If the minimum value of entropy is found in a deterministic system, a stochastic one should present higher values. The variation of entropy can be observed in the graph of Figure 7, which presents a particular case, where it is assumed probability mass function given by

$$p(X = x_i) = \begin{cases} p(X = 1) = \rho \\ p(X = 0) = 1 - \rho, \end{cases} \tag{4}$$

with ρ as a value in the closed interval $[0; 1]$.

As a measure of uncertainty, entropy presents small values when measuring ordered processes, and its value increases when measuring unordered processes. At the extremes of Figure's 7 curve, ρ values either 0 or 1, and the probability distribution $p(X = x_i)$ (from Equation 4) is either given by

$$\begin{cases} p(X = 0) = 0 \\ p(X = 1) = 1 \end{cases} \quad or \quad \begin{cases} p(X = 0) = 1 \\ p(X = 1) = 0. \end{cases} \tag{5}$$

The value of entropy in these points is 0, which is obtained by

$$H(X) = \; - 0 \cdot log(0) - 1 \cdot log(1) \qquad or \qquad H(X) = \; - 1 \cdot log(1) - 0 \cdot log(0). \tag{6}$$

Considering now the peak in the curve in Figure 7, the maximum value of entropy is at the point where $\rho = 0.5$. In such case, the probability distribution of $p(X = x_i)$ is given by

$$\begin{cases} p(X = 0) = 0.5 \\ p(X = 1) = 0.5, \end{cases} \tag{7}$$

and the value of entropy is obtained by

$$\begin{aligned} H(X) &= -2(0.5 \cdot log(0.5)) \\ &= -log(0.5) \\ &= 1. \end{aligned} \tag{8}$$

Figure 7: Variation of entropy values according to the probability ρ. $H(X)$ reaches its minimum value (0.0) when the probability ρ is either 0 or 1, which are deterministic cases with minimum uncertainty. $H(X)$ increases for non-deterministic configurations (ρ different than 0 or 1). It reaches its maximum value (1.0) when ρ is 0.5, which is the case with maximum uncertainty.

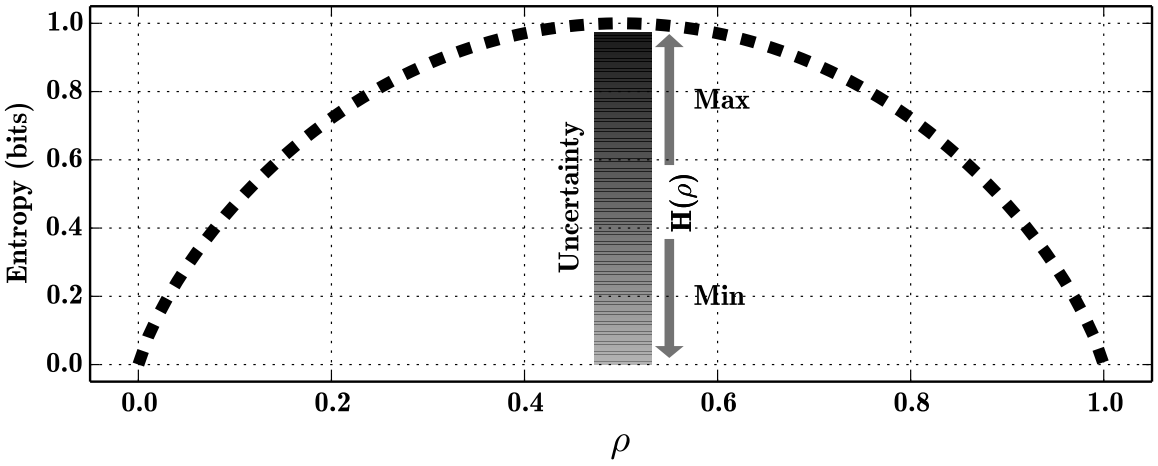

Source: generated by the author.

Joint and Conditional Entropy

Joint entropy represents the amount of uncertainty in the association of two processes (COVER; THOMAS, 2006). It is an extension of the entropy concept from a single variable to a multivariate scenario.

Consider a pair of random variables: X with alphabet $\mathcal{X}$, and Y with alphabet $\mathcal{Y}$. Also, consider that these variables present a joint probability distribution $p(x, y) = Pr\{X = x; Y = y\}, x \in \mathcal{X}$ and $y \in \mathcal{Y}$. The joint entropy $H(X, Y)$ is defined to be calculated by the following expression

$$H(X, Y) = -\sum_{x \in \mathcal{X}} \sum_{y \in \mathcal{Y}} p(x, y)\ log\ p(x, y). \tag{9}$$

Conditional entropy $H(X|Y)$ is the residual uncertainty in the association of two processes when the state of one is given. Considering the same random variables X and Y, and their conditional probability $p(X|Y)$ (WALPOLE et al., 2014), Equation 1 can be rewritten, and the conditional entropy $H(X|Y)$ can be found by the mathematical manipulation

$$\begin{aligned} H(X|Y) &= \sum_{y \in \mathcal{Y}} p(y)\ H(X|Y = y) \\ &= -\sum_{y \in \mathcal{Y}} p(y) \sum_{x \in \mathcal{X}} p(x|y)\ log\ p(x|y) \end{aligned}$$

$$
\begin{aligned}
&= -\sum_{y\in\mathcal{Y}}\sum_{x\in\mathcal{X}} p(y)\frac{p(x,y)}{p(y)}\ log\ p(x|y) \\
&= -\sum_{x\in\mathcal{X}}\sum_{y\in\mathcal{Y}} p(x,y)\ log\ \frac{p(x,y)}{p(y)},
\end{aligned}
\tag{10}
$$

where $p(x|y)$ is the conditional probability of X given Y.

3.1.1 Relative Entropy and Mutual Information

Relative entropy was introduced by Kullback and Leibler (KULLBACK; LEIBLER, 1951 apud COVER; THOMAS, 2006), and it is used to measure the divergence between two probability distributions. Relative entropy shows the inability of assuming that a random variable is represented by a probability distribution q, instead of p, the variable's real probability distribution.

The Kullback-Leibler divergence between q and p, for a random variable X with alphabet $\mathcal{X}$, is given by the following equation

$$
D(p||q) = \sum_{x\in\mathcal{X}} p(x)\ log\frac{p(x)}{q(x)}. \tag{11}
$$

When both probabilities are zero, $p(X = x_i) = 0$ and $q(X = x_i) = 0$, the value of relative entropy is zero. This is due to the fact that

$$
\begin{cases}
\lim\limits_{q\to 0^+}\lim\limits_{p\to 0^+} p\ log\ q = 0 \\
\lim\limits_{q\to 0^-}\lim\limits_{p\to 0^+} p\ log\ q = 0 \\
\lim\limits_{q\to 0^+}\lim\limits_{p\to 0^-} p\ log\ q = 0 \\
\lim\limits_{q\to 0^-}\lim\limits_{p\to 0^-} p\ log\ q = 0.
\end{cases}
\tag{12}
$$

In such case, the approximation q is close to the real probability distribution, p, thus the divergence 0.

In the case when only p is zero, $p(X = x_i) = 0$ and $q(X = x_i) \neq 0$, relative entropy value is zero again, because of the fact that

$$
\begin{cases}
\lim\limits_{p\to 0} p\ log\ p = 0 \\
0 \cdot log\ q = 0.
\end{cases}
\tag{13}
$$

However, in the case when only q is zero, $p(X = x_i) \neq 0$ and $q(X = x_i) = 0$, the value of relative entropy tends to infinity, because of

$$
\lim_{q\to 0^+}\ p\ log\ q = -\infty. \tag{14}
$$

In this case, the approximation q is not a good representation.

Mutual Information

Mutual information is a particular case of relative entropy (COVER; THOMAS, 2006). It calculates the Kullback-Leibler divergence between the joint probability distribution of two random variables, and $p(x, y) = p(x)p(y)$, which is the case when X and Y are independent of each other (WALPOLE et al., 2014).

For a pair of random variables X and Y, that have alphabets $\mathcal{X}$ and $\mathcal{Y}$, and joint probability distribution $p(x, y)$, the mutual information between X and Y is given by the equation

$$I(X;Y) = \sum_{x \in \mathcal{X}} \sum_{y \in \mathcal{Y}} p(x, y)\ log \frac{p(x, y)}{p(x)p(y)}, \tag{15}$$

where $p(x)$ and $p(y)$ are the marginal probability mass functions of $p(x, y)$.

Comparing Equations 11 and 15, we see that the joint distribution $p(x, y)$ is the correspondent of p. In the same way, $p(x)p(y)$ is the correspondent of q. Thence, the value of mutual information will be zero when X and Y are independent from each other. This is due to the relation

$$p(x, y) = p(x)p(y) \Rightarrow log \frac{p(x)p(y)}{p(x)p(y)} = log\ 1 = 0. \tag{16}$$

Furthermore, by comparing $p(x, y)$ and $p(x)p(y)$, mutual information can be used to investigate independences between random variables.

Delayed Mutual Information

Time-delayed mutual information is a way of use time sweepings to investigate interaction delays and also measures the information shared between processes. It has been widely used to build models for propagations. Examples are the modeling of structural dynamics in complex systems (NICHOLS, 2006) and the study of respiratory muscles (ALONSO et al., 2007).

Delayed mutual information is a method based on Equation 15, with the addition of a time-lag τ. It can be represented by the following equation

$$DMI(X;Y) = I(X;Y^{\tau}), \tag{17}$$

where τ stands for the time-delay between process X and Y. Therefore, for two processes X and Y, with a time-lag τ, the delayed mutual information is given by

$$\begin{aligned} DMI(X;Y) &= I(X;Y^{\tau}) \\ &= \sum_{x \in \mathcal{X}} \sum_{y \in \mathcal{Y}} p(x, y^{\tau})\ log \frac{p(x, y^{\tau})}{p(x)p(y^{\tau})}. \end{aligned} \tag{18}$$

Relation Between Entropy and Mutual Information

Equation 15 can be rewritten in terms of entropy and conditional entropy as follows

$$\begin{aligned} I(X;Y) &= \sum_{x\in\mathcal{X}}\sum_{y\in\mathcal{Y}} p(x,y)\ log\frac{p(x,y)}{p(x)p(y)} \\ &= \sum_{x\in\mathcal{X}}\sum_{y\in\mathcal{Y}} p(x,y)\ log\frac{p(x|y)}{p(x)} \\ &= -\sum_{x\in\mathcal{X}}\left[\sum_{y\in\mathcal{Y}} p(x,y)\right] log\ p(x) - \left[-\sum_{x\in\mathcal{X}}\sum_{y\in\mathcal{Y}} p(x,y)\ log\ p(x|y)\right] \\ &= -\sum_{x\in\mathcal{X}} p(x)\ log\ p(x) - H(X|Y) \\ &= H(X) - H(X|Y). \end{aligned} \tag{19}$$

This shows that MI is the reduction in the uncertainty of X given the knowledge of Y (COVER; THOMAS, 2006). The same mathematical manipulation can be done to consider the entropy of Y as follows

$$log\frac{p(x,y)}{p(x)p(y)} = log\frac{p(y|x)}{p(y)} \Rightarrow I(X;Y) = H(Y) - H(Y|X). \tag{20}$$

By manipulating Equation 19, it is also possible to represent the relation between mutual information and the joint entropy as

$$\begin{aligned} I(X;Y) &= H(X) - H(X|Y) \\ &= H(X) - \left[-\sum_{x\in\mathcal{X}}\sum_{y\in\mathcal{Y}} p(x,y)\ log\ p(x|y)\right] \\ &= H(X) + \sum_{x\in\mathcal{X}}\sum_{y\in\mathcal{Y}} p(x,y)\ log\frac{p(x,y)}{p(y)} \\ &= H(X) - \sum_{y\in\mathcal{Y}}\left[\sum_{x\in\mathcal{X}} p(x,y)\right]\ log\ p(y) - \left[-\sum_{x\in\mathcal{X}}\sum_{y\in\mathcal{Y}} p(x,y)\ log\ p(x,y)\right] \\ &= H(X) - \sum_{y\in\mathcal{Y}} p(y)\ log\ p(y) - H(X,Y) \\ &= H(X) + H(Y) - H(X,Y). \end{aligned} \tag{21}$$

Furthermore, the relation between entropy and mutual information can be expressed by the following expression

$$H(X,Y) = H(X) + H(Y) - I(X;Y), \tag{22}$$

which is illustrated by the Venn's diagram in Figure 8.

Figure 8: Venn's diagram exhibiting the relation between entropy and mutual information. $I(X;Y)$ is the reduction in the uncertainty of Y given the knowledge of X. The Venn's diagram represents graphically the relation presented by Equation 22.

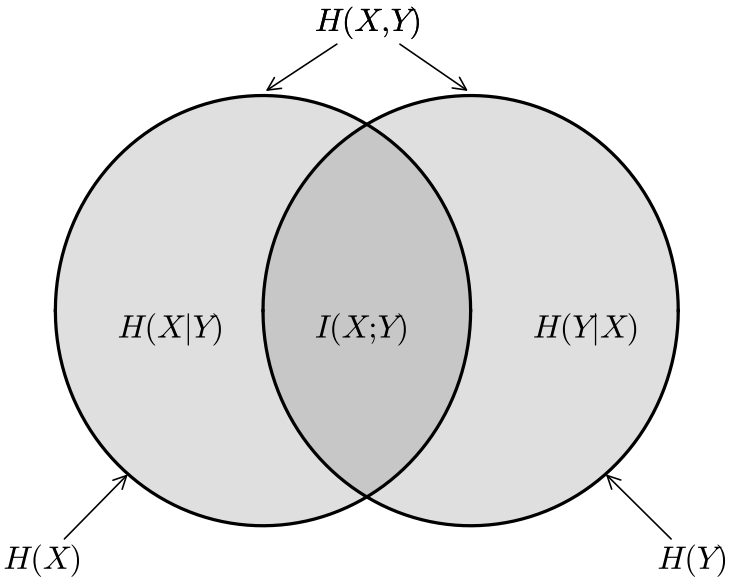

Source: generated by the author based on Cover and Thomas (2006).

3.1.2 Data Processing Inequality

The data processing inequality (COVER; THOMAS, 2006) is a property of mutual information. It is used to show that manipulations in the data cannot improve the inferences made from it. Data processing inequality is based on the chain rule for mutual information, which expands this concept to cases with three or more variables (COVER; THOMAS, 2006).

For a set of n random variables, $X1, ..., Xn$, the chain rule for mutual information (COVER; THOMAS, 2006) states that the MI between them and a process Y is given by the following expression

$$I(X_1, X_2, ..., X_n; Y) = \sum_{i=1}^{n} I(X_i; Y|X_{i-1}, X_{i-2}, ...). \tag{23}$$

Now, let us suppose three processes, X, Y, and Z, that are organized as follows

$$X \to Y \to Z, \tag{24}$$

where Z is conditionally independent of X, if Y is given, i.e., the conditional probability distribution of Z depends only on Y. According to the chain rule, the mutual information between processes X, Y, and Z is given by

$$\begin{aligned} I(X;Y,Z) &= I(X;Z) + I(X;Y|Z) \\ &= I(X;Y) + I(X;Z|Y). \end{aligned} \tag{25}$$

The assumption of Equation 24 that X and Z are conditionally independent if Y is given leads to $I(X;Z|Y) = 0$. Rewriting the expression of Equation 25 with the consideration of conditional independence we have

$$\begin{aligned} I(X;Z) + I(X;Y|Z) &= I(X;Y) + I(X;Z|Y) \\ &= I(X;Y). \end{aligned} \tag{26}$$

As a result, the data processing inequality (COVER; THOMAS, 2006) states that for three random variables, configured as in Equation 24, mutual information presents the following property

$$X \rightarrow Y \rightarrow Z \quad \Rightarrow \quad I(X;Z) \leq I(X;Y) \tag{27}$$

3.2 Transfer Entropy

Transfer entropy (SCHREIBER, 2000) is an information theoretical measure that has been widely applied to data analysis. Its range of applications may vary from the identification of propagation directions in a chemical process (BAUER et al., 2007) to the analysis of large-scale industrial faults (YANG; XIAO, 2012).

It is capable of identifying dependencies and independencies between two random variables (VICENTE et al., 2011), and also of investigating causal relations (BARNETT; BARRETT; SETH, 2009). In neuroscience, transfer entropy applications helped to describe dependencies between regions of the brain (WIBRAL; VICENTE; LINDNER, 2014).

Transfer entropy was defined by Schreiber as the amount of information that a past state of a process X contains about an observation of Y, given the past state of the process Y. Generically, it can be defined (WIBRAL; VICENTE; LINDNER, 2014) as

$$TE(X \rightarrow Y) = I(X^-; Y|Y^-) \tag{28}$$

where X^- e Y^- are past states of processes X and Y, respectively.

Schreiber (2000) proposed TE to be calculated by the following expression

$$TE(X \rightarrow Y) = \sum_{x \in \mathcal{X}} \sum_{y \in \mathcal{Y}} p(y_{n+1}, y_n^{(k)}, x_n^{(l)}) \log \frac{p(y_{n+1}|y_n^{(k)}, x_n^{(l)})}{p(y_{n+1}|y_n^{(k)})} \tag{29}$$

where $p(x)$ and $p(y)$ are probability mass functions for processes X and Y, with alphabets $\mathcal{X}$ and $\mathcal{Y}$. Also, $y_n^{(k)}$ stands for k past states of Y, and $x_n^{(l)}$ stands for l past states of X.

Kantz and Schreiber (2004) argued that the number of samples that have to be considered to represent the past of a variable can be found with delayed mutual information of the variable with itself. Considering k as this number of samples, the time lag of interest is found in the first local minimum of

$$I(Y;Y^d) = \sum_{y \in \mathcal{Y}} p(y, y^d) \log \frac{p(y, y^d)}{p(y)p(y^d)}, \tag{30}$$

where Y_d stands for d previous samples of Y.

Silchenko et al. (2010) showed that the time-delay between two random variables could be found in the maximum peak of information transfer. DTE is defined then as a measure in function of a time-delay β. This means that time-delayed transfer entropy is the one presented by Schreiber, with the addition of a time lag (WIBRAL et al., 2013). Thus, the time-delay τ between processes X and Y is given by the DTE between them and the past of Y_k^τ

$$\begin{aligned} DTE(X \to Y) &= TE(X_\beta \to Y) \\ &= \sum_{x \in \mathcal{X}} \sum_{y \in \mathcal{Y}} p(y, y_\alpha, x_\beta) \log \frac{p(y|y_\alpha, x_\beta)}{p(y|y_\alpha)}, \end{aligned} \tag{31}$$

where k stands for the number of samples that represent the past of the variable Y.

3.2.1 Delayed Transfer Entropy and Delayed Mutual Information

Both measures, the time-delayed mutual information and the time-delayed transfer entropy, base themselves on information shares. However, a single share of information is not enough to determine a cause-effect relation. This is a well-known fact that represents a common mistake. A single information share does not mean that one process is the cause of the other since *"correlation does not imply causality"* (DEMARIE-DREBLOW, 1991).

Delayed mutual information is a symmetric measure (SCHREIBER, 2000), which means that for two random variables, X and Y, the time-delayed mutual information measured from X to Y is same that the one measured from Y to X,

$$I(X; Y^\tau) = I(Y^\tau; X). \tag{32}$$

As a result, time-delayed mutual information is not capable of differentiating between information that is exchanged and information that is simply and only shared.

Although DTE also investigates information shares, it is not a symmetric measure (SCHREIBER, 2000). For two process X and Y, the DTE measured from X to Y is not the same as the one measured from Y to X,

$$DTE(X \to Y^\tau) \neq DTE(Y^\tau \to X). \tag{33}$$

DTE identifies and eliminates the information that is simply and only shared between two processes, and that is not useful to establish a cause-effect relation. Therefore, DTE is capable of identifying information exchanges. Moreover, as a result, it is capable of properly establish causal relations between random variables (BARNETT; BARRETT; SETH, 2009).

Figure 9 illustrates the relation between DTE and delayed mutual information. It can be seen that time-delayed mutual information uses all the knowledge common to both processes. It can be represented as

$$I(X; Y^{\tau}) : X \cap Y^{\tau}, \tag{34}$$

where the symbol $\cap$ represents the intersection of the processes information.

In Figure 9 it can also be seen that time-delayed transfer entropy uses the same variables in the same time-lag as the delayed mutual information, i.e., X and Y^{τ}. However, it also uses the past of the target variable (Y_k^{τ}) to remove the effect of the shared information. DTE can be represented as

$$TE(X \rightarrow Y) : (X \cap Y^{\tau}) - (X \cap Y^{\tau} \cap Y_k^{\tau}), \tag{35}$$

where the symbol $\cap$ represents the intersection of the variables information.

The major difference between these two measures is that transfer entropy finds and removes the non-cause-effect shared information. This can be found in the intersection of process X and Y^{τ} with Y_k^{τ}, as can be seen in Figure 9.

3.3 Surrogate Time Series

The point of maximum coherence between two time-series is found when their phases are synchronized (YANG et al., 2013). To validate results of information theoretical measures, one possible approach is to exchange one signal by synthetic data, and then repeat the experiments. Such approach can use the technique of surrogate time series (SCHREIBER; SCHMITZ, 2000). Examples of information theoretical measures used along with surrogate are delayed mutual information (JIN; LIN; HALLETT, 2010) and DTE (PAPANA; KUGIUMTZIS; KYRTSOU, 2014).

The word "surrogate" stands for something that is used instead of something else. In the case of surrogate signals, the synthetic data used is randomly generated, i.e., it is a noisy signal, but it also presents some characteristics of the signal that it is taking place (DOLAN; SPANO, 2001). A surrogate time series presents the same power spectrum as the original signal, but these two signals are uncorrelated.

One technique of generation for surrogate time series consists of making changes in the signal's phase while keeping its power spectrum and probability distribution. Such technique is the "Iterative Amplitude Adjusted Fourier Transform", that was proposed by Schreiber and Schmitz (2000), and improved later by Venema, Ament and Simmer (2006). It consists on a phase shifting of the original signal, where the phase is substituted by a Gaussian white noise in an iterative process, which is illustrated in Figure 10.

Figure 9: Relation between time-delayed mutual information at the top left, time-delayed transfer entropy at the top right, and samples of X and Y at the bottom. Venn's diagrams show that delayed mutual information takes all the shared information X and Y^τ, while DTE disregards the information shared by X, Y^τ, and its past Y_k^τ. While the delayed mutual information is a symmetric measure, DTE is not.

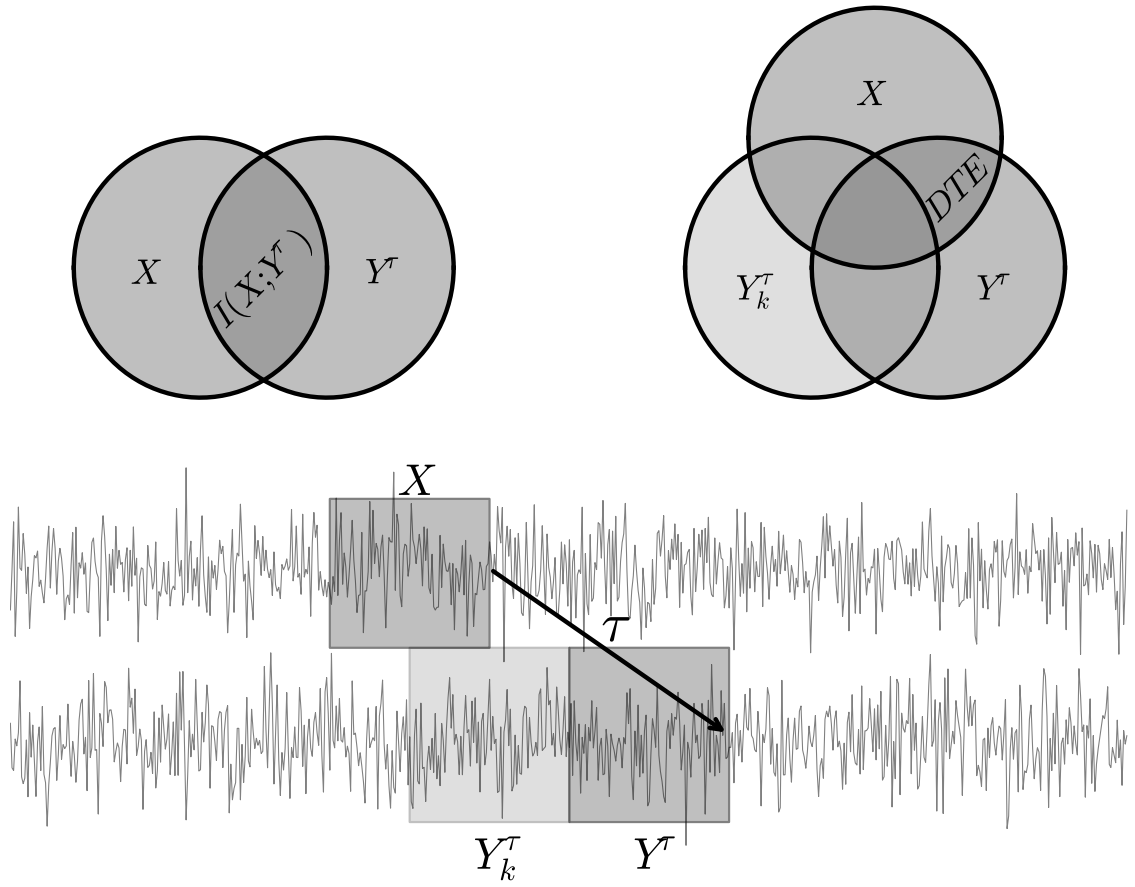

Source: generated by the author based in Endo (2014).

Suppose a signal x that is represented in both domains, time and frequency, by $x(t)$ and $X(j\omega)$. Also, suppose a surrogate signal x_S, that is represented in time and frequency by $x_S(t)$ and $X_S(j\omega)$. These signals present the following relations

$$\begin{cases} x(t) \leftrightarrow X(j\omega) = A(\omega)e^{j\phi(\omega)}, \\ x_S(t) \leftrightarrow X_S(j\omega) = A(\omega)e^{j\phi(GWN)}, \end{cases} \qquad p(x_S) = p(x) \tag{36}$$

where $p(x)$, and $p(x_S)$ are the probability mass functions of the variables x, and x_S; the signals' power spectrum is given by $A(j\omega)$; and $e^{j\phi(\omega)}$ and $e^{j\phi(GWN)}$ stand for the signals' phase.

Figure 10: Illustration of the surrogate time series generation with the "Iterative Amplitude Adjusted Fourier Transform" method (VENEMA; AMENT; SIMMER, 2006; SCHREIBER; SCHMITZ, 2000). The signals in the left are presented in the time-domain, and their respective probability distributions are shown at the right. Signal A is the one for which the surrogate data will be generated. Signals B and C are two surrogates of A, but they present a different probability distribution. Signal D is other surrogate data of A that presents a probability distribution similar to A, differently of B and C.

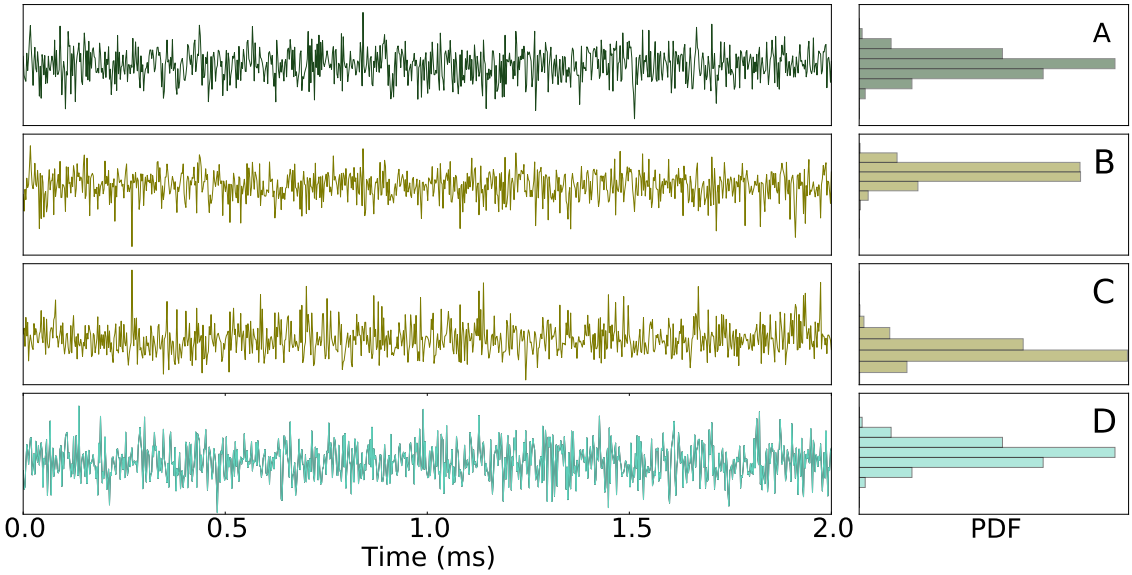

Source: generated by the author.

Chapter 4

Methodology and Parameter Estimation

This chapter presents the methodology used for study the FeCO, starting by explaining how the data was analyzed. Section 4.2 shows the simulation process and the methods for the generation of synthetic data. In the last section, the method of parameters estimation for the interaction between two random variables are presented.

The data analysis started by measuring the time intervals between two consecutive spikes. This is an old technique named inter-spike interval (REICH et al., 2000), which is widely used in neuroscience (SCHWALGER; DROSTE; LINDNER, 2015; BROWN; KASS; MITRA, 2004; ROCHA et al., 2007). It is possible, with such technique, to model the spike signal using models different than the ones that only represent the occurrence or not of a spike, i.e., to use not only a Poisson counting process (LEGENDY; SALCMAN, 1985).

Parameters obtained with inter-spike interval are used to assemble models of survival functions (LAWLESS, 2011). These are from a branch of Statistics that models the time until the occurrence of an event (KLEIN; MOESCHBERGER, 2003). Examples of applications include the fields of reliability, with the failure of a system (ACHCAR; MOALA, 2015); and medicine, with a patient longevity (MACKENZIE et al., 2014). Survival models are also used to analyze the remission time (CABRERO et al., 2015), which is the time spent between two occurrences of the same types of events (BEWICK; CHEEK; BALL, 2004), or two spikes in the case of FeCO signals.

Section 4.2 will review the methods from what synthetic data can be generated. The section starts by providing a review of a set of packages for generating random data for a given probability distribution, and also for a graph-based model. Moreover, to describe the process of data generation, it proceeds by presenting some properties of transforms between random variables.

Such transforms are based on the *inverse transform method* (ZIO, 2013), which, based on uniformly distributed random samples, allows data to be generated following any probability distribution. Such method is represented by an algorithm in Section 4.2, and

an example the process of data generation for three graphs, each one composed of three nodes in a different topological configuration.

In the last section, the "Estimation of Joint Probability Distributions" is presented. This is a method that intends to infer parameters for the interaction of two random processes. Such method is a hill-climbing algorithm (RUSSELL et al., 2003), which is based on a combination of mutual information and surrogate data. This method of estimation intends to find one joint probability distribution that fits a given specification of mutual information and to do that, it carefully changes the values of cells inside a joint probability table, while the required value of mutual information is not achieved.

4.1 Data Analysis

To investigate the neuronal responses of FeCO, a method that measures the time between two spikes, the *inter-spike intervals (ISI)* (SCHWALGER; DROSTE; LINDNER, 2015), was employed in this study. As the name suggests, the inter-spike interval is the amount of time spent between two consecutive spikes (ROCHA et al., 2007).

The methods to calculate the inter-spike interval are illustrated by Figure 11, where the intervals between spikes are measured from a spiking time series, and they are also represented in a graphic, where the abscissa represents the value of the time interval.

One usage of ISI is to measure time intervals between spikes and try to fit them into a probability distribution (CHEN et al., 2009). As a consequence, it is possible to obtain parameters that describe the occurrence of spikes from these distributions. For this research, the most relevant parameters are the mean time between spikes (**MTBS**), and their correspondent confidence intervals, which will help to characterize different responses of the FeCO in Chapter 5.

The mean time between spikes is given in units of $ms/spike$, and it is the inverse of the spike rate λ ($spike/ms$). These parameters can be obtained by a Poisson counting process (LEGENDY; SALCMAN, 1985), and they can be used to fit an exponential survival function $s(T = t)$. This will represent the probability of non-occurrence of another spike at a time $T = t$, given the past occurrence of a spike. The survival model will be formally introduced in the sequence.

4.1.1 Survival Analysis

Survival models are statistical representations that aim to model the behavior of sets of individuals, according to the time interval necessary for an event to happen (COLLETT, 2003). The FeCO response can be modeled with survival functions if considering the time between occurrences of events (BEWICK; CHEEK; BALL, 2004), here represented by ISI and the MTBS.

Figure 11: Methods for calculating the inter-spike interval (ISI) and its parameters. At the top, the time interval τ_i between two consecutive spikes is measured for each pair of spikes, in the spiking signal $x(t)$. The interest here is in the values of the time intervals, which are represented in the abscissa τ_i, at the bottom's left. Also, it is possible to obtain parameters to describe the occurrence of spikes, by fitting ISI values in any statistical function, such as an exponential distribution, or a Gaussian, as in the bottom's right.

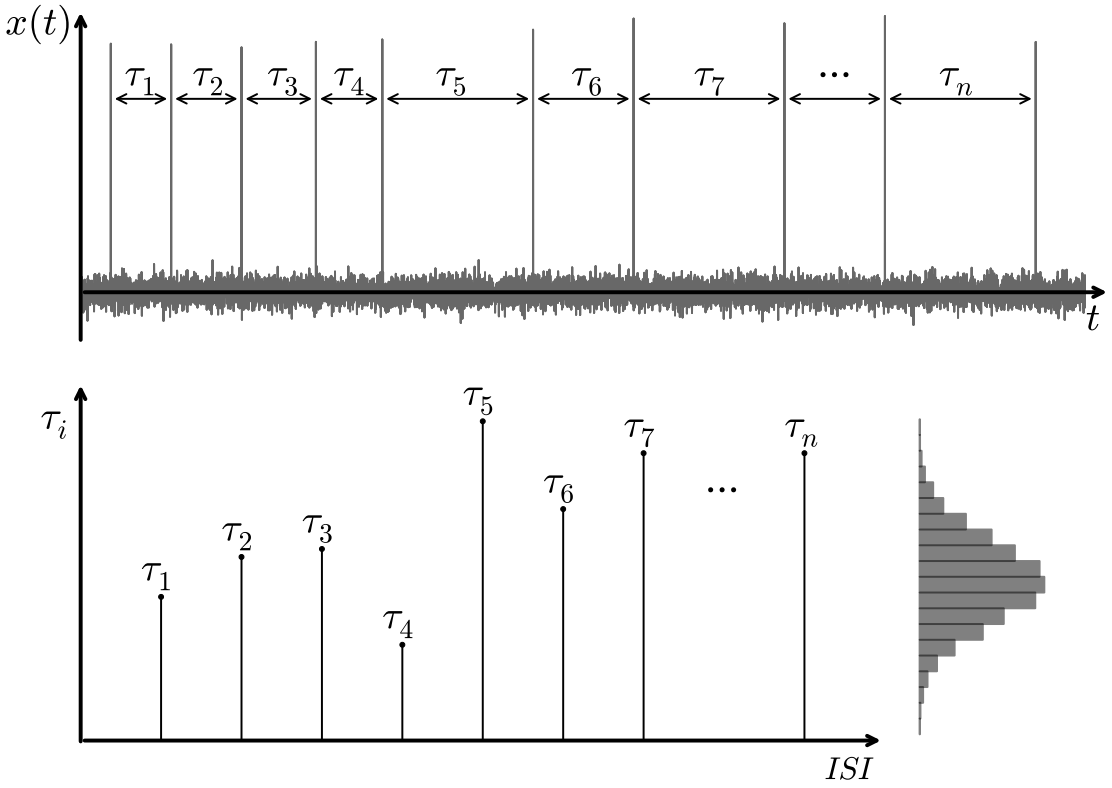

Source: generated by the author.

A survival time variable (T) is a non-negative random variable representing the time until an event occurs (KLEIN; MOESCHBERGER, 2003). If $f(t)$ accounts for the probability density function of T, and $F(t)$ its cumulative distribution function, then the survival function $S(t)$ is defined as follows

$$S(t) = Pr(T \geq t) = 1 - F(t) = \int_t^\infty f(x)dx, \tag{37}$$

which represents the probability of an event do not occur during the time t.

A concept related to the survival variable T is the hazard function $h(t)$, that is defined as

$$h(t) = \lim_{\Delta t \to 0} \frac{P(t \leq T < t + \Delta t | T \geq t)}{\Delta t}. \tag{38}$$

The hazard function represents the instantaneous rate of a given event occurs at the time t (KLEIN; MOESCHBERGER, 2003). If $\Delta t \to 0$,

$$P(t \leq T < t + \Delta t) \to f(t), \tag{39}$$

and, based on the conditional probability rule (WALPOLE et al., 2014), the Equation 38 can be rewritten as

$$h(t) = \frac{f(t)}{S(t)}. \tag{40}$$

In the experiments that recorded the FeCO signals, the excitation was a Gaussian white noise with a fixed bandwidth. If the spike rate is considered to be constant, due to a fixed input, consequently, the hazard function is also constant. For such case, it is reasonable to assume an exponential distribution,

$$f(t) = \lambda e^{-\lambda t} = \mu e^{-\frac{t}{\mu}}, \tag{41}$$

with a survival function

$$S(t) = e^{-\lambda t} = e^{-\frac{t}{\mu}}, \tag{42}$$

where λ is the spike rate (spikes/ms), and μ the distribution mean (ms/spike) (HARRELL, 2013), i.e., the mean time between spikes.

4.2 Synthetic Data

To generate random numbers for a specific probability distribution, there are several packages available. Examples include the "*Random Number Generation*" in Matlab[1] and R[2]; the function *rand* in C/C++[3] language; the class "*Random*" in Java[4]; and the function '*random*' in Python[5].

This language, Python, also presents libraries for scientific computation (MILLMAN; AIVAZIS, 2011; OLIPHANT, 2007). Among its packages, one of the most relevant for scientific applications is *scipy* (WALT; COLBERT; VAROQUAUX, 2011), which includes the library *numpy* that has a set of different functions to generate random numbers for specific probability distributions.

The variety of computational packages to generate random samples shows that this is a largely exploited area. However, despite the complexity of any package or library presented, all process of generation are based on the same method. The method referred is the *inverse transform method* which can be found in Zio (2013), Peebles, Read and Read (2001), and Li et al. (1994) studies.

[1] "Random Number Generation". [Online] Accessed in 23 June, 2016. Available at: `http://www.mathworks.com/help/matlab/random-number-generation.html?requestedDomain=www.mathworks.com`.

[2] "Random Number Generation". [Online] Accessed in 23 June, 2016. Available at: `https://stat.ethz.ch/R-manual/R-devel/library/base/html/Random.html`.

[3] "C Reference function rand generate a random number". [Online] Accessed in 23 June, 2016. Available at: `https://www.codingunit.com/c-reference-stdlib-h-function-rand-generate-a-random-number`.

[4] "Class Random". [Online] Accessed in 23 June, 2016. Available at: `https://docs.oracle.com/javase/8/docs/api/java/util/Random.html`.

[5] "9.6. random – Generate pseudo-random numbers". [Online] Accessed in 23 June, 2016. Available at: `https://docs.python.org/2/library/random.html`.

The inverse transform method is mathematical manipulation of probability and cumulative distribution functions (PEEBLES; READ; READ, 2001), that aims to generate random numbers from any probability distribution. In other words, this method transforms a random variable X, with a probability distribution $f(x) = p(X = x)$, in another random variable Y, with probability distribution $f(y) = p(Y = y)$. Such transform ($Y = T\{X\}$) is obtained by

$$f(y) = F(x), \tag{43}$$

where $F(x) = p(X \leq x)$ stands for the cumulative probability distribution function of the random variable X (WALPOLE et al., 2014).

Transform of an Uniform Variable into an Exponential

To exemplify the transformation process with the inverse transform method, this example presents the calculations for a random variable X to Y. Suppose that X is uniformly distributed, $X \sim U(a, b)$, and Y is exponentially distributed, $Y \sim Exp(\lambda)$. The cumulative probability distributions of X ($F(x)$), and the probability distribution of Y are given by

$$\begin{cases} F(x) = \frac{x-a}{b-a} \\ f(y) = \lambda e^{-\lambda y}. \end{cases} \tag{44}$$

The transform $F(x) = f(y)$ is then given by

$$\begin{aligned} \frac{x-a}{b-a} &= \lambda \exp^{-\lambda y} \\ ln\left(\frac{x-a}{b-a}\right) &= ln\left(\lambda e^{-\lambda y}\right) \\ ln\,(x-a) - ln\,(b-a) &= ln\,(\lambda) - \lambda y \\ y &= -\left(\frac{ln\,(\lambda) + ln\,(b-a) - ln\,(x-a)}{\lambda}\right). \end{aligned} \tag{45}$$

For a specific case where $a = 0$, $b = 1$, and $\lambda = 1$, the transform is given by the following expression

$$y = -ln\,(x)\,. \tag{46}$$

4.2.1 Transform of Discrete Random Variables

The inverse transform method allows to analytically finding the expression that satisfies $Y = T\{X\}$, as shown by the example above. However, there are cases without an analytical solution, which require an approach with numerical methods (PEEBLES; READ; READ, 2001). Such approach is the same done for taking samples from discrete random variables, and for these cases, an algorithm can do the task of finding the association function.

A random variable X has probability distribution given by $f(x) = p(X = x_j) = p_j$, where $\sum_j p_j = 1$. Another random variable R has values inside the closed interval $[0; 1]$, and its probability distribution $p(R = r)$ is uniformly distributed. Supposing that a sample r of the variable R is taken, and used as a seed in the procedures

$$X = \begin{cases} x_0, & r < p_0 \\ x_1, & p_0 \leq r < p_0 + p_1 \\ \vdots & \vdots \\ x_j, & \sum_{i=0}^{j-1} p_i \leq r < \sum_{i=0}^{j} p_i, \end{cases} \tag{47}$$

the resultant number x_j will be a sample of the random variable X, that follows the probability distribution $f(x)$.

The extension of the inverse transform method for discrete random variables can be resumed by the following expression

$$P\{X = x_j\} = P\left\{\sum_{i=0}^{j-1} p_i \leq r < \sum_{i=0}^{j} p_i\right\} = p_j. \tag{48}$$

Additionally, the generation of n samples for the random variable X with probability distribution $p(x)$ can be done by following the steps of Algorithm 1.

Algorithm 1 The inverse transform method (based on a uniform probability distribution) to sample a random variable X according to a probability distribution $p(x)$.

Require: n: number of samples; P: probability distribution; bin: values of X.

```
for j=0; j<n; j++ do
    r ← rand(0;1);
    i ← 0;
    while r>0 do
        r -= P(i);
        i++;
    end while
    data(j) ← bin(i)
end for
return data
```

4.2.2 Data Generation for Graph Based Models

The same procedures of Algorithm 1, if properly adapted, can be used to generate data for graph-based models. Consider the three random variables X, Y, and Z, and the topological organization of case A, both presented in Figure 12. A result of the network's topology is that the nodes X and Z are conditionally independent, if Y is given, and the following relations can be established

$$\begin{cases} p(X|Y, Z) = p(X|Y) \\ p(Z|X, Y) = p(Z|Y). \end{cases} \tag{49}$$

The relations of Equation 49 imply that in the case of network A if a state of Y is given, it is possible to infer the states of Z and X without additional knowledge. As a consequence, one could take a sample of Y as an independent variable, and then infer the states of the other nodes.

In the same way, if the state of X is given in the network B, it is possible to infer the states of Y and Z, because

$$\begin{cases} p(Y|X,Z) = p(Y|X) \\ p(Z|X,Y) = p(Z|X). \end{cases} \tag{50}$$

However, in some cases, it could not be possible to infer the node state, only with the knowledge about the state of one variable. This is the case of the nodes Y of topology A, the node X of topology B, and also the three nodes of topology C.

To sample data from those nodes, it is necessary to observe the networks' topology and make an approximation by considering the conditional probability only between two nodes. For example, in topology A, if X is known, and Y and Z are not, an approximation of the probability of Y can be achieved by considering Y and Z as independent, then

$$p(Y|X,Z) = p(Y|X). \tag{51}$$

This is an approximation that allows the sampling of Y, without the need for the knowledge of Z. For the cases of networks A and B, this could be done differently by sampling Z and Y as independent variables, respectively. However, in network C, it is necessary to consider the existence of connections between each pair of nodes, and the described proceedings are needed. Moreover, to fully exploit the methods, the next three examples will describe the process of data sampling for three graph-based models.

Figure 12: Setup with three graphs to exemplify the process of data generation. Each case is composed of three nodes, and the respective configuration of its arrows refers to the test of the algorithms (see the Section 5.1 of Chapter 5).

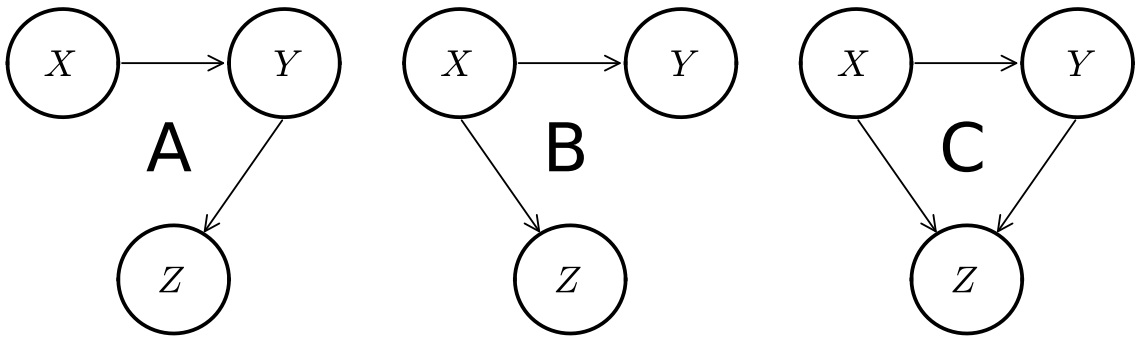

Source: generated by the author.

Network A

The topological relations of nodes X, Y, and Z presented in network A shows that X and Z are conditionally independent if the state of Y is given. This implies in the following relations

$$p(X, Z|Y) = p(X|Y)p(Z|Y) \Rightarrow \begin{cases} p(X|Y, Z) = p(X|Y) \\ p(Z|Y, X) = p(Z|Y). \end{cases} \tag{52}$$

The simulation process can start in any one of the network's nodes, and, based on the relations for topology A in Equation 52, and there are three ways to proceed when generating data in such topology. These ways are:

- start from node X, pass trough Y, and reach to Z:

$$X \rightarrow Y \rightarrow Z;^{6}$$

- start from node Y and reach both nodes, X and Z:

$$X \leftarrow Y \rightarrow Z;$$

- start from node Z, pass trough Y, and reach X:

$$Z \rightarrow Y \rightarrow X.$$

When starting from node X, the fist step is to sample a value of it using $p(X)$ as P in Algorithm 1. The state of Y (the next node) can be inferred by the conditional probability of Y given X, which is calculated by the equation

$$p(Y|X) = \frac{p(X, Y)}{P(X)}, \tag{53}$$

where $p(X, Y)$ is the joint probability distribution of Y and X.

The conditional probability of Y given X presents values inside the closed interval $[0.0; 1.0]$, and the sum of its elements is equal to one. Hence, $p(Y|X)$ can be used as the entry P in Algorithm 1, which will sample data for the connection $X \rightarrow Y$.

In the same way, the sample of node Z will be taken by considering the sampled state of Y, which will be the parameter to calculate the conditional probability of Z, given the state of Y. By following the same steps of the Y generation, the next state of Z can be inferred by $p(Z|Y)$.

If the simulation starts from node Y, its state will be inferred based on its probability distribution by Algorithm 1. Two conditional probabilities will be computed for X and

[6] Differently from the arrows of Figure 12, these arrows only represent the order that data is sampled, i.e., first X, then Y, and then Z. They do not represent a connection, or a cause-effect relation between the variables.

Z, given the state of Y: $p(X|Y)$, and $p(Z|Y)$, and these will generate data for X and Z according to the given state of Y.

In the last case, when the simulation starts from node Z, data following its probability distribution will be sampled with Algorithm 1. The conditional probability $p(Y|Z)$ will be calculated to sample data for node Y, and also $p(X|Y)$ will be computed to sample data for X.

Network B

Based on the topological relations for nodes X, Y, and Z presented in network B, the nodes Y and Z are conditionally independent if X is given. This implies in the following relations

$$p(Y, Z|X) = p(Y|X)p(Z|X) \Rightarrow \begin{cases} p(Y|X, Z) = p(Y|X) \\ p(Z|Y, X) = p(Z|X). \end{cases} \tag{54}$$

The simulation process can start in any one of the network's nodes, and, based on the relations for topology B in Equation 54, and there are three ways to proceed when generating data in such topology. These ways are:

- ❏ start from node X, and reach both Y and Z:

$$Y \leftarrow X \rightarrow Z;$$

- ❏ start from node Y, pass trough X, and reach Z:

$$Y \rightarrow X \rightarrow Z;$$

- ❏ start from node Z, pass trough X, and reach Y:

$$Z \rightarrow Y \rightarrow X.$$

When starting from node X, the fist step is to sample a value of it using $p(X)$ as P in Algorithm 1. The states of Y and Z can be inferred by the conditional probability of Y and Z given X, $p(Y|X)$ and $p(Z|X)$, respectively.

If the simulation starts from node Y, its state will be inferred Algorithm 1 following $p(Y)$. The conditional probability $p(X|Y)$ will be calculated to sample data for node X, and then, $p(Z|X)$ will also be computed to sample data for Z.

In the last case, when the simulation starts from node Z, data that follow its probability distribution will be sampled with Algorithm 1. The conditional probability $p(X|Z)$ will be calculated to sample data for node X. And $p(Y|X)$ will also be computed to sample data for Y.

Network C

Differently then cases A and B, the topological order of nodes X, Y, and Z in case C does not show conditional independencies. For this configuration, the simulation can also start in anyone of the network's nodes. However, conditional probabilities have to consider the states of two variables, i.e.,

$$p(X|Y,Z), \qquad p(Y|X,Z), \qquad \textit{and} \qquad p(Z|X,Y). \tag{55}$$

In this specific case, there are six different ways of generate data, which are:

- ❏ start from node X, pass trough Y, and use both to generate Z:

$$Y \leftarrow X \rightarrow Z \leftarrow Y;$$

- ❏ start from node X, pass trough Z, and use both to generate Y:

$$Z \leftarrow X \rightarrow Y \leftarrow Z;$$

- ❏ start from node Y, pass trough X, and use both to generate Z:

$$X \leftarrow Y \rightarrow Z \leftarrow X;$$

- ❏ start from node Y, pass trough Z, and use both to generate X:

$$Z \leftarrow Y \rightarrow X \leftarrow Z;$$

- ❏ start from node Z, pass trough Y, and use both to generate X:

$$Y \leftarrow Z \rightarrow X \leftarrow Y;$$

- ❏ start from node Z, pass trough X, and use both to generate Y:

$$X \leftarrow Z \rightarrow Y \leftarrow X.$$

When starting from node X, the fist step is to sample a value of it using $p(X)$ as P in Algorithm 1. If passing trough Y, the probability $p(Y|X)$ is calculated and a sample of Y is taken. With these values, the probability $p(Z|X,Y)$ is computed, and a sample of Z is taken.

In the same way, if starting from X and passing trough Z before Y, the probability $p(Z|X)$ is calculated, and a sample of Z is taken. With these values, the probability $p(Y|X,Z)$ is computed, and a sample of Y is taken.

Now, if the simulation starts from node Y, data that follows its probability distribution will be sampled with Algorithm 1. If passing through X before Z, the conditional

probability $p(X|Y)$ (or $p(Z|Y)$ if passing through Z before X) will be calculated to sample data for node X (or Z). And, then, $p(Z|X,Y)$ (or $p(X|Y,Z)$) will also be computed to sample data for Z (or X).

In the last case, the state of Z will be inferred with its probability distribution by Algorithm 1. If passing through X before Y the conditional probability $p(X|Z)$ (or $p(Y|Z)$ if passing through Y before X) will be calculated to sample data for node X (or Y). And, then, $p(Y|X,Z)$ (or $p(X|Y,Z)$) will also be computed to sample data for Y (or X).

4.3 Estimation of Joint Probability Distributions

Methods for data generation require the variables probability distributions, and some multivariate cases (some graph-based models for example) require the joint probability distribution is also required. If working with actual time series, it is possible to build a two-dimensional histogram (n-dimensional if working with n variables) using, for example, the function *histogramdd* from the SciPy library. However, in simulated environments, which usually is not filled with actual data, or in applications with non-simultaneous recordings, it is not possible to build a histogram.

The problem of determining a joint probability distribution brings the need for a method capable of estimating it, and for that, an iterative hill-climbing algorithm is proposed. Such method is Algorithm 2, which requires the probability distributions of the associated variables, and their mutual information, which will show their "level" of interaction.

The proper value of mutual information for Algorithm 2 can be estimated with surrogate time series. In general, for any value of mutual information above zero, the interaction between random variables is assumed as not independent. However, it is also known that a single information share (which could be the case of mutual information) does not imply a causality relation. It is expected then that processes could present a low level of mutual information even if they are not related. Therefore, surrogate time series are used to find a threshold for mutual information.

To estimate a joint probability distribution for two random variables X and Y, the simulation starts by taking their marginal probability distributions $p(x)$ and $p(y)$. It builds the initial joint distribution which is $p(x,y) = p(x)p(y)$, and presents mutual information equal to zero.

Simulation proceeds, by generating the signals $x(t)$ and $y(t)$ with Algorithm 1. It generates a set of n pairs of surrogate data $x_S(t)$ and $y_S(t)$, according to the method presented by Venema, Ament and Simmer (2006). The surrogate data is used in the calculation of the mutual information threshold MI_T. Such threshold is the value of mutual information above what X and Y are considered as not being independent. MI_T

is found in the maximum value of mutual information between the pairs $[x_S(t), y_S(t)]$.

With MI_T and the initial joint distribution, the simulation proceeds to change the values inside $p(x, y)$. The first step is to randomly choose two numbers $i1$ and $j1$ from the range of bins in the joint distribution matrix, choosing a cell $p(x_{i1}, y_{j1})$, which will have a percentage of its mass removed. Another number $j2$ is randomly selected to choose a cell $p(x_{i1}, y_{j2})$, which will have the mass removed from $p(x_{i1}, y_{j1})$ added to its contents.

The process described keeps the sum over the joint probability distribution equal to one. It also keeps the marginal $p(x)$ intact, but the marginal $p(y)$ is changed. To correct that, another number $i2$ is randomly chosen selecting a cell $p(x_{i2}, y_{j2})$, and the same mass removed from $p(x_{i1}, y_{j1})$ will be removed from it. To complete the process, the simulation will add the removed mass to a fourth cell $p(x_{i2}, y_{j1})$. These proceedings assure that the sum over the joint distribution and also none of the marginals are changed.

The proceedings of moving some mass into the joint probability function are repeated while the mutual information, calculated over the joint probability distribution, is smaller than MI_T. After finding a joint probability distribution that fits the requirements, any software or even the Algorithm 1 can be used for generating data.

Algorithm 2 A method for estimate a joint probability distribution based on mutual information and surrogate data.

Require: p: probability distribution; ρ: acceptable error; b: number of bins; n: number of surrogates; STS: generates surrogate data; I: mutual information; ABS: absolute value; *rand*: sample a random number in an specified interval.

1: p(x,y) $\leftarrow$ p(x)p(y)
2: Generate samples of X and Y: $[x(t), y(t)]$
3: Generate surrogate data for X and Y:

$$\begin{array}{cccc} x_{S1} & \leftarrow STS(x(t)), & y_{S1} & \leftarrow STS(y(t)) \\ \vdots & \vdots & \vdots & \vdots \\ x_{Sn} & \leftarrow STS(x(t)), & y_{Sn} & \leftarrow STS(y(t)) \end{array}$$

4: Calculate the mutual information between each pair of surrogate:

$$\begin{array}{ccc} mi_1 & \leftarrow & I(x_{S1}, y_{S1}) \\ \vdots & & \vdots \\ mi_n & \leftarrow & I(x_{Sn}, y_{Sn}) \end{array}$$

5: Calculate the threshold MI_T: $MI_T \leftarrow max(mi_1, ..., mi_n)$
6: Calculate the error: $\gamma \leftarrow ABS(I(p(x, y)) - MI_T)$
7: **while** $\gamma > \rho$ **do**
8: Cell to remove mass:

$$i1 \leftarrow rand_{int}(0; b_X)$$
$$j1 \leftarrow rand_{int}(0; b_Y)$$

9: Cell to add mass: $j2 \leftarrow rand_{int}(0; b_Y)$
10: Mass to be removed: $\delta \leftarrow p(x_{i1}, y_{j1}) \cdot rand(0; 1)$
11: Change the joint probability distribution:

$$p(x_{i1}, y_{j1}) - = \delta$$
$$p(x_{i1}, y_{j2}) + = \delta$$

12: Cell to balance mass: $i2 \leftarrow rand_{int}(0; b_X)$
13: Change the joint probability distribution:

$$p(x_{i2}, y_{j2}) - = \delta$$
$$p(x_{i2}, y_{j1}) + = \delta$$

14: Calculate the new mutual information: $MI \leftarrow I(p(x, y))$
15: **if** $ABS(MI - MI_T) < \gamma$ **then**
16: $\gamma \leftarrow MI$
17: **else**
18: reject changes
19: **end if**
20: **end while**
21: return p(x,y)

Chapter 5

Measures, Simulations and Results

The proposal of this work is to analyze signals from the insect proprioceptor system. We observed some properties of the neuronal signals to identify patterns and different types of responses. However, due to experimental limitations, it was not possible to record signals from every region of interest. As a consequence, measures of connectivity between such regions could not be done, and to try to solve this problem we presented Algorithm 2 in Chapter 4.

The first section intends to validate our algorithms. We applied them to three test cases, estimated the joint probability distributions, generated data and learned inferred nodes connections from the synthetic data. To infer the existence or the absence of connections we used DTE. These results were presented in the 7th edition of an international congress and in the 21st edition of a national congress, both in 2016[1].

In the second and third sections, we analyzed the neuronal signals. Firstly, we looked into the FeCO spiking rates and modeled it with statistical functions investigating differences in the neuronal responses. After that, we applied DTE in the signals investigating time delays and analyzing the influence of excitation in sensory neurons responses. Both analysis allowed us to identify different neuronal responses, and also to classify the experiments by the observed characteristics. These results were presented in the 9th edition of an international congress in 2016[2].

In the fourth section, we applied our algorithms together with the neuronal signals assuming the existence of connections between sensory neurons. We assumed two models and inferred parameters for their joint probability distributions with Algorithm 2. We used some data from the original experiments as a seed in the process of data generation, and compared the synthetic data with the expected result (the original signal). Currently, a paper with that analysis is being prepared for submission.

[1] See Subsections 5.5.2 and 5.5.3.
[2] See Subsection 5.5.1

5.1 Algorithms Validation

For each case, the joint probability distribution was calculated between each pair of nodes with Algorithm 2. The simulation generated synthetic data for each node in each configuration, and DTE between each pair of nodes was calculated.

Figure 13: Three graphs designed to test the simulation algorithms, test cases: A, B, and C. Each one has three nodes: one GWN and two $Spk1$ and $Spk2$. The simulation of these test cases follows the procedures presented for the networks in Figure 12.

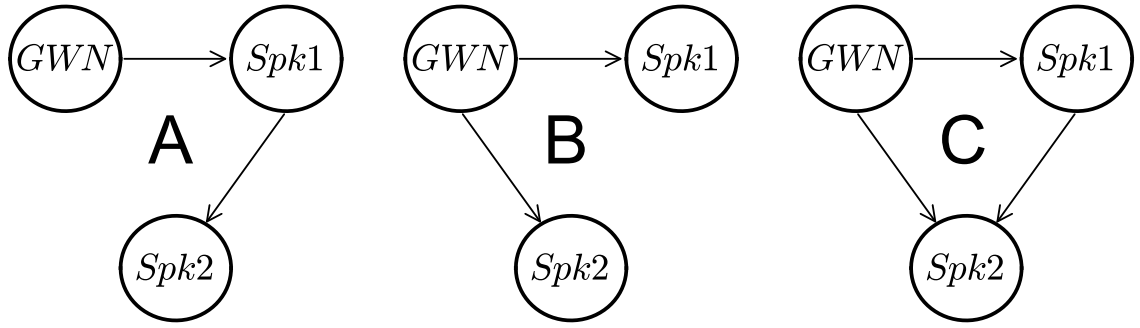

Source: Generated by the author.

5.1.1 Simulation

A discrete probability distribution was assigned to each node. The Shannon's entropy associated with the GWN was $H(GWN) = 4.39$; and for $Spk1$ and $Spk2$, the entropy was: $H(Spk1) = H(Spk2) = 3.93$. The number n of surrogates generated was thirty, and mutual information measured the pairs $[x_{Si}; y_{Si}]$.

With the set of surrogates, the threshold for mutual information was found to be $MI_T = 0.1$. However, a value ten times greater was assumed, to increase the information share. Such modification respected the maximum mutual information between nodes, which was 3.93.

Simulation proceeded to the calculation of joint probability distributions $p(GWN, Spk)$ and $p(Spk1, Spk2)$. The first represents connections $GWN \leftrightarrow Spk1$ and $GWN \leftrightarrow Spk2$, and the second represents connection $Spk1 \leftrightarrow Spk2$.

Then, a data set with $900k$ samples per node was generated for each case in Figure 13. Additionally, a time delay was inputted between the time series of each node. These time delays are listed in Table 3, where the character "—" is presented when there is no connection.

Table 3: Artificial time delays (units in ms) inserted between the nodes of the graphs presented in Figure 13. The character "—" is inserted when there is no connection between two nodes.

Connection	A	B	C
$GWN \rightarrow Spk1$	50	50	50
$GWN \rightarrow Spk2$	—	70	70
$Spk1 \rightarrow Spk2$	20	—	20

5.1.2 Network Reconstruction

After simulating the three test cases, the next step was to reconstruct the networks from the synthetic data. In the reconstruction process, we used DTE that was chosen to validate our algorithms with a different metric (mutual information was used in the simulation).

According to Wibral et al. (2013), the time-delay between two random variables can be found in the maximum value of their DTE. Therefore the curve $time \times DTE$ should present a peak at the point of interaction, and as a consequence, the existence of such peak indicates a connection.

Tests were divided in three steps, each one testing the existence and the directionality of a specific connection between two nodes. This was done for each topology presented in Figure 13, and the connections tested in each step were

$$I: \begin{cases} GWN \rightarrow Spk1 \\ GWN \leftarrow Spk1 \end{cases} \quad II: \begin{cases} GWN \rightarrow Spk2 \\ GWN \leftarrow Spk2 \end{cases} \quad III: \begin{cases} Spk1 \rightarrow Spk2 \\ Spk1 \leftarrow Spk2. \end{cases}$$

Tests for $GWN \leftrightarrow Spk1$

As can be seen in Figure 13, the three cases presented a connection between such nodes. It was expected that Figure 14 would suggest the existence of such connection in cases A, B, and C.

At the top row of Figure 14, graphics A, B, and C present curves with peaks at 20 ms, while the graphics of the bottom do not present such peaks. The combination of the existence and the absence of peaks in graphics of Figure 14 points to the directionality of connection $GWN \leftrightarrow Spk1$.

The directionality is characterized by peaks in DTE when the target variable is $Spk1$. In the same way, the absence of peaks when the target variable is GWN reinforces that there is no information flow from $Spk1$ to GWN. Therefore, the direction of information flow is from node GWN to the node $Spk1$, and there is a connection between GWN and $Spk1$ with 50 ms of time delay.

Figure 14: DTE between nodes GWN and $Spk1$. The top row shows the measures calculated when the target variable was $Spk1$, testing the existence of an information flow from GWN to $Spk1$. The bottom row shows the measures calculated when the target variable was GWN, testing the existence of an information flow from $Spk1$ to GWN. Peaks in the top row and their absence in the bottom row show that the direction of information flow is $GWN \rightarrow Spk1$ with 20 ms of time delay.

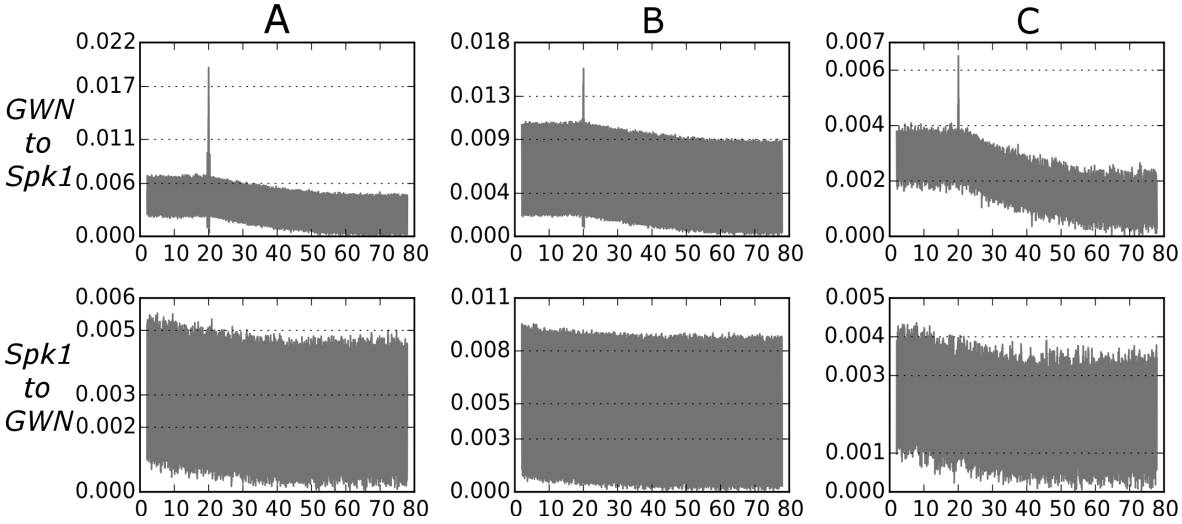

Source: Generated by the author.

Tests for $GWN \leftrightarrow Spk2$

As can be seen in the topologies from Figure 13, in case A there is no connection between nodes GWN and $Spk2$, while cases B and C present a connection between these nodes. It was expected that Figure 15 would suggest the existence of such connections in cases B, and C, and none connection in case A.

At the top row of Figure 15, graphics B, and C present curves with peaks at 70 ms. Graphic A also presents a peak at the same time. However, the difference between its amplitude and the ground noise is lower than the one presented by other peaks. Although the peak found in graphic A should be considered, its low amplitude brings doubts about the existence of such connection.

Like in Figure 14, the graphics of the bottom of Figure 15 do not present any peak, and this points to the connection's directionality. These results suggest the existence of a connection when measuring the information flow from node GWN to node $Spk2$ in cases B and C. It is possible to state that the direction of the information flow is $GWN \rightarrow Spk2$, with 70 ms of time delay in cases B and C. However, without additional knowledge, the connection between GWN and $Spk2$ in case A is kept in the dark.

Tests for $Spk1 \leftrightarrow Spk2$

As can be seen in Figure 13, cases A and C present a connection between these nodes, while case B does not present it. Thus, it was expected that the measures presented in

Figure 15: Delayed transfer entropy measures between GWN and $Spk2$. The top row shows the measures calculated when the target variable was $Spk2$, testing the existence of an information flow from GWN to $Spk2$. The bottom row shows the measures calculated when the target variable was GWN, testing the existence of an information flow from $Spk2$ to GWN. Peaks in the top row of cases B and C, and their absence in the bottom row, show that the direction of information flow is $GWN \rightarrow Spk2$, with 70 ms of time delay. However, there is doubt about the peak of case A because of its low amplitude.

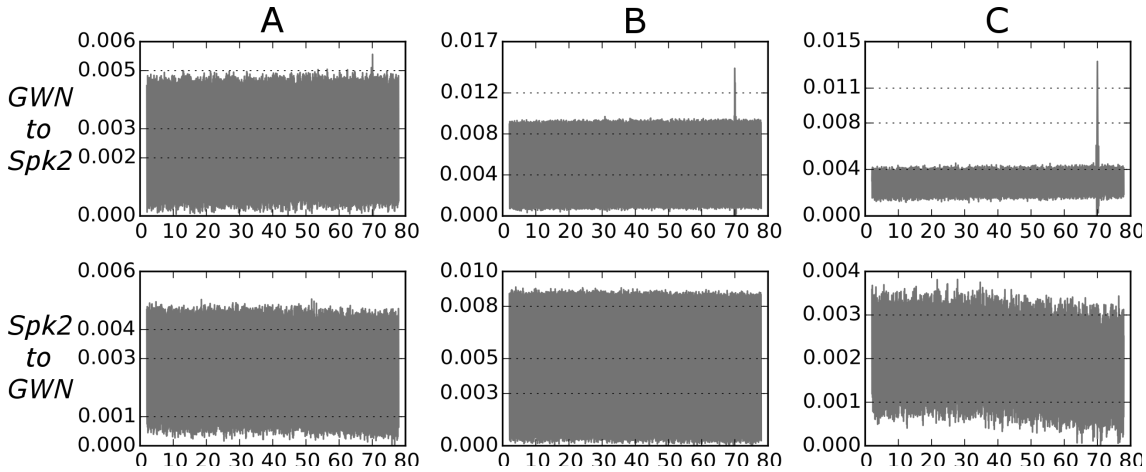

Source: Generated by the author.

Figure 16 would suggest the existence of such connection in cases A and C, and none in case B.

At the top row of Figure 16, graphics A and C present curves with a peak at 50 ms, and the graphic B presented no one. In the bottom of the figure, the graphics of DTE did not present peaks. The combination of the existence and the absence of peaks, in graphics A and C of Figure 16, points to a directionality in the connection.

The directionality is characterized by peaks in the DTE when the target variable was $Spk2$. In the same way, the absence of peaks when the target variable was $Spk1$, reinforces that there is no information flow from $Spk2$ to $Spk1$. Hence, the direction of information flow is from the node $Spk1$ to node $Spk2$ in cases A and C.

Peaks in the Network Reconstruction

The peaks found in the process of reconstruction confirmed the connections of networks from Figure 13, with an exception for connection $GWN \rightarrow Spk2$ in the first topology. However, as can be seen in Figures 14, 15, and 16, the referred peak is too small when compared with others. To properly compare the peaks, we compiled their difference to the maximum ground noise of each case in Table 4, where the character "—" is presented when no connection was found.

Figure 16: Delayed transfer entropy measures between $Spk1$ and $Spk2$. The top row shows the measures calculated when the target variable was $Spk2$, testing the existence of an information flow from $Spk1$ to $Spk2$. The bottom row shows the measures calculated when the target variable was $Spk1$, testing the existence of an information flow from $Spk2$ to $Spk1$. Peaks in the top row, and their absence in the bottom row, show that the direction of information flow is $GWN \rightarrow Spk1$, with 50 ms of time delay.

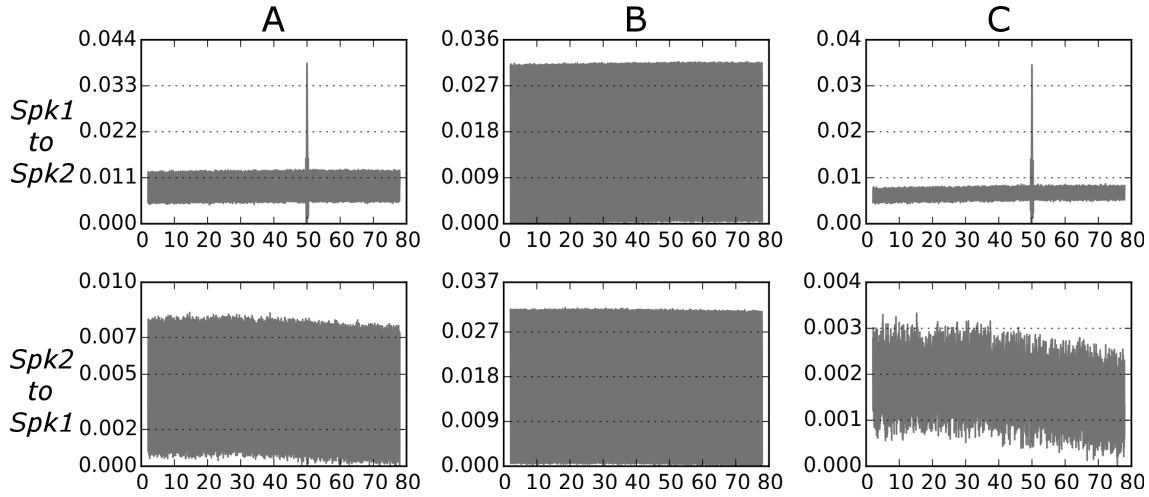

Source: Generated by the author.

Table 4: Percentage difference between the DTE peaks and the maximum of the ground noise for each connection tested. The character "—" is inserted when no peak was found.

Connection	A	B	C
$GWN \rightarrow Spk1$	17.30%	5.51%	3.75%
$Spk1 \rightarrow GWN$	—	—	—
$GWN \rightarrow Spk2$	0.84%	5.48%	10.00%
$Spk2 \rightarrow GWN$	—	—	—
$Spk1 \rightarrow Spk2$	14.62%	—	9.79%
$Spk2 \rightarrow Spk1$	—	—	—

5.2 Mean Time Between Spikes

As introduced in Chapter 4, the inter spike intervals were measured for each experiment in Table 2. ISI were used in the calculation of statistical parameters, that followed the usual equations for an exponential variable (WALPOLE et al., 2014) with mean μ and variance σ^2 given by the estimators

$$\widehat{\mu} = \sum_{i=1}^{n} \frac{x_i}{n} = \frac{1}{\lambda} \qquad and \qquad \widehat{\sigma}^2 = \sum_{i=1}^{n} \frac{(x_i - \mu)^2}{n-1}, \tag{56}$$

and also confidence intervals for the mean (or the mean time between spikes) given by

$$IC = \bar{x} \pm t_{n-1,\frac{\alpha}{2}} \frac{S_X}{\sqrt{n}}, \tag{57}$$

where S_X is the sample standard deviation; t comes from a t-distribution; and α is the probability of an error in the estimation of the interval.

We measured ISI in each sample presented in Table 2, calculated their MTBS and the correspondent confidence intervals considering an $\alpha = 5\%$. These results are presented in Tables 5 and 6. Additionally, Figures 17 and 18 provide a visualization of the MTBS distribution.

MTBS for 27 Hz Signals

Table 5 presents the MTBS and their confidence intervals measured for each sample with the 27 Hz excitation. MTBS varies from 16.92 ms to 85.10 ms, presenting a mean of 36.33 ms, and a normalized standard deviation of 47.81%. Such dispersion of the MTBS (normalized standard deviation close to 50%) leads us to consider the possibility of different neuronal responses when the same excitation is applied in the locust apodeme. These considerations are reinforced by the histogram presented in Figure 17, that shows two groups of MTBS separated by a gap.

Table 5: MTBS and their respective confidence intervals for experiments with 27 Hz.

Experiment ID	Animal Number	Lower Endpoint	MTBS	Top Endpoint
ID–701	18	15.78 ms	16.92 ms	18.04 ms
ID–702	18	58.14 ms	62.23 ms	66.17 ms
ID–766b[3]	22	41.75 ms	44.38 ms	47.00 ms
ID–773	22	34.95 ms	36.82 ms	38.69 ms
ID–774	22	26.14 ms	28.71 ms	31.27 ms
ID–778	22	45.32 ms	49.10 ms	52.88 ms
ID–781	22	49.99 ms	53.26 ms	56.53 ms
ID–923	25	58.15 ms	62.16 ms	66.18 ms
ID–926	25	23.73 ms	24.66 ms	25.58 ms
ID–929	25	24.05 ms	25.35 ms	26.65 ms
ID–932	25	19.51 ms	20.32 ms	21.12 ms
ID–934	25	22.46 ms	23.49 ms	24.52 ms
ID–937	25	78.81 ms	85.10 ms	91.38 ms
ID–945	25	30.45 ms	32.63 ms	34.49 ms
ID–948	25	46.85 ms	49.83 ms	52.80 ms
ID–1004	26	24.45 ms	25.56 ms	26.68 ms
ID–1006	26	31.42 ms	33.06 ms	34.68 ms
ID–1008	26	28.42 ms	29.89 ms	31.35 ms
ID–1010	26	21.72 ms	22.67 ms	23.61 ms
ID–1013	26	22.00 ms	23.00 ms	24.00 ms
ID–1016	26	21.95 ms	23.17 ms	24.40 ms
ID–1019	26	25.68 ms	26.91 ms	28.15 ms
Mean			36.33 ms	
Standard Deviation			17.37 ms	
Normalized Standard Deviation			47.81%	

Figure 17: Histogram for the MTBS of 27 Hz signals presented in Table 5. The presence of a gap suggests the existence of different groups of response.

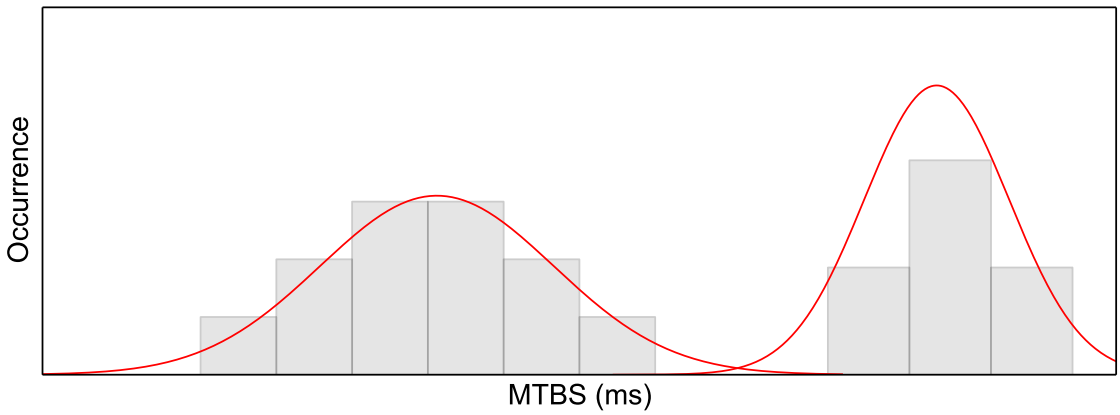

Source: Generated by the author.

MTBS for 58 Hz Signals.

Table 6 presents the MTBS and their confidence intervals measured for each sample with the 58 Hz excitation. MTBS varies from 12.69 ms to 51.9ms, presenting a mean of 26.16 ms, and a normalized standard deviation of 40.15%. Although this dispersion of the MTBS is smaller than the one presented by the 27 Hz signals, it also suggests the possibility of different neuronal responses, as the histogram of in Figure 18 suggests.

Figure 18: Histogram for the MTBS of 58 Hz signals presented in Table 6. The presence of a gaps suggests the existence of different groups of response.

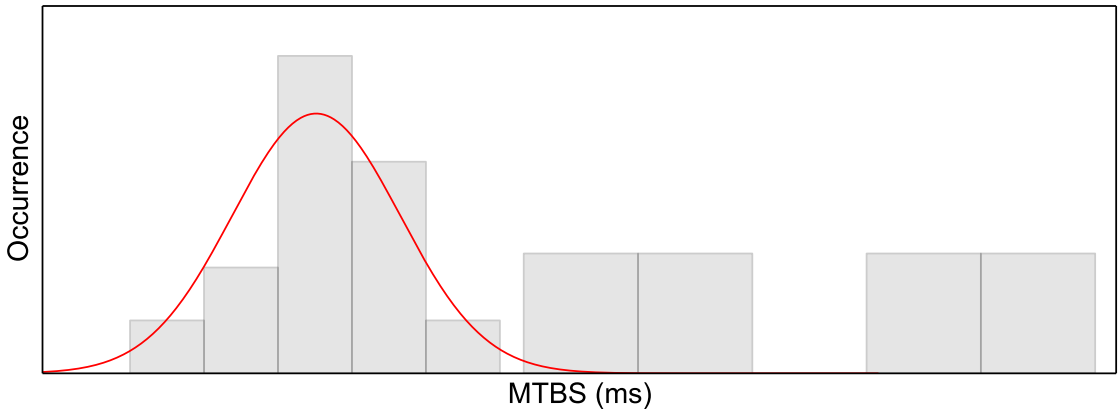

Source: Generated by the author.

[3]The label b in this signal refers to one of its half, the one with the 27 Hz excitation (see about the entry 58/27 for experiment ID–766 in Table 2).

Table 6: MTBS and their respective confidence intervals for experiments with 58 Hz.

Experiment ID	Animal Number	Lower Endpoint	MTBS	Top Endpoint
ID–765	22	12.69 ms	13.67 ms	14.65 ms
ID–766a	22	27.36 ms	29.17 ms	30.98 ms
ID–767	22	28.86 ms	30.17 ms	31.47 ms
ID–780	22	22.96 ms	24.12 ms	25.28 ms
ID–924	25	24.84 ms	25.79 ms	26.74 ms
ID–927	25	20.51 ms	21.32 ms	22.13 ms
ID–930	25	17.87 ms	18.57 ms	19.27 ms
ID–935	25	19.40 ms	20.15 ms	20.90 ms
ID–946	25	22.43 ms	23.46 ms	24.48 ms
ID–1003	26	51.90 ms	54.12 ms	56.33 ms
ID–1005	26	22.56 ms	23.46 ms	24.36 ms
ID–1009	26	19.67 ms	20.43 ms	21.19 ms
ID–1011	26	19.58 ms	20.37 ms	21.16 ms
ID–1012	26	45.06 ms	46.69 ms	48.32 ms
ID–1014	26	18.33 ms	19.03 ms	19.73 ms
ID–1015	26	37.91 ms	39.35 ms	40.78 ms
ID–1017	26	19.53 ms	20.35 ms	21.18 ms
ID–1020	26	19.88 ms	20.69 ms	21.5 ms
Mean			26.16 ms	
Standard Deviation			10.50 ms	
Normalized Standard Deviation			40.15%	

5.2.1 Models for the Time Between Spikes

With MTBS calculated, we used them to build models with survival functions for the time spent between spikes. We found two groups of signals in the experiments with 27 Hz excitation (Figure 17), and for 58 Hz we found three groups (Figure 18). However, for 58 Hz experiments, we calculated only the statistics of one group, because each one of the other two was composed by only two samples.

We present the parameters of the models in Table 7, and the curves of each model with the respective confidence interval is presented in Figure 19. The assumption of different spiking rates is reinforced by the curves as their confidence intervals are non-overlapping.

Table 7: Parameters of the models for the time spent between spikes.

Group	Lower Endpoint	μ (ms/spike)	Top Endpoint
27 Hz			
1st	24.01	27.26	30.52
2nd	46.49	53.49	60.50
58 Hz			
1st	19.43	21.47	23.51

Figure 19: Models for the time spent between consecutive spikes. Survival probability functions for the two groups of neuronal response in the 27 Hz experiments (top), and for one group in the 58 Hz (bottom).

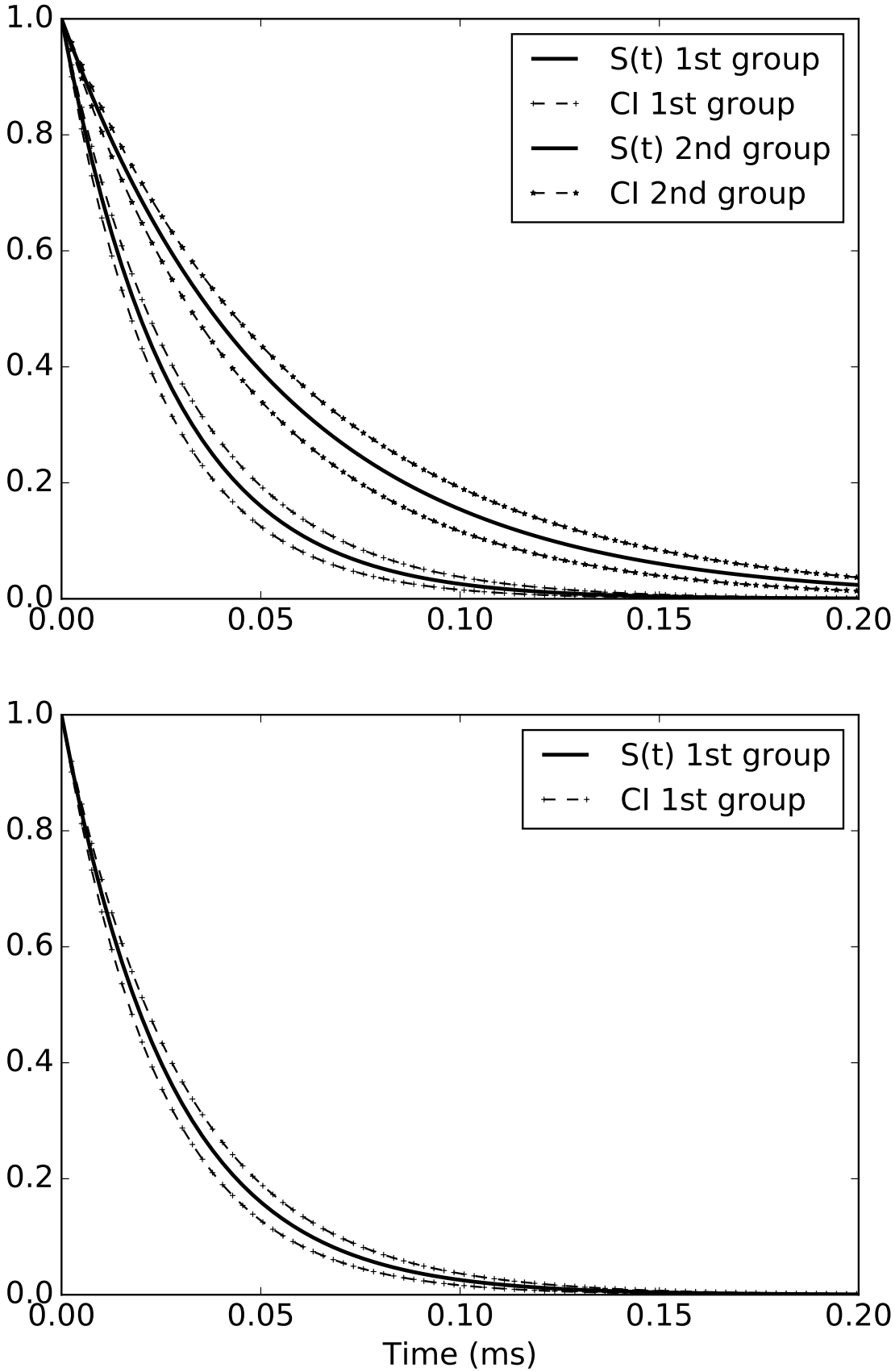

Source: Generated by the author.

5.3 Delayed Transfer Entropy

To find time-delays and determine interactions among the signals, we calculated the DTE between the two pairs: *excitation - filtered excitation*; and *filtered excitation - sensory neuron.*

The time delay for the pair *excitation - filtered excitation* is known to be given by the filter equation, since it adds a specific time delay to the signal (MANAL; ROSE, 2007). For this reason, the delay found with DTE for this pair can be used as a reference measure.

5.3.1 Reference Measures for Delayed Transfer Entropy

With the help of DTE, we calculated the time delay between the pair 200 Hz and 27 Hz (or 58 Hz) for each sample in Table 2. The results of these measurements are presented in Tables 8 and 9, and their respective curves in Figures 20 and 21.

DTE 200 Hz → 27 Hz

For a cutoff frequency (f_c) of 27 Hz, the filter adds a fixed and well known time delay (MANAL; ROSE, 2007), which is given by the equation

$$\begin{aligned} delay &= \frac{0.416}{f_c} \\ &= \frac{0.416}{27} \\ &= 15.41 \cdot 10^{-3}\ s. \end{aligned} \tag{58}$$

Hence it is expected that the DTE between the pair 200 Hz and 27 Hz would present a time delay of 15.41 ms.

The DTE curves obtained for the pair 200 Hz → 27 Hz are presented in Figure 20, and the time delays in Table 8. The measures present a normalized standard deviation of 1.67%, and their mean diverges 4.22% from the expected time delay. This diversion is acceptable because the cutoff frequency was manually adjusted during the experiments.

DTE 200 Hz → 58

In the same way as for the 27 Hz signals, the filter adds a fixed and well known time delay for a cutoff frequency of 58 Hz (MANAL; ROSE, 2007), which is 7.17 ms. The DTE curves obtained for the pair 200 Hz → 58 Hz are presented in Figure 21, and the time delays in Table 9. They present a normalized standard deviation of 3.4%, and their mean diverges 7.53% from the expected time delay. Again, such diversion is acceptable because the cutoff frequency was manually adjusted during the experiments.

Figure 20: Reference measures for DTE (200 Hz → 27 Hz).. DTE curves shows a peak around 15.00 ms, with a low variation in the measured delay as can be seen in Table 8.

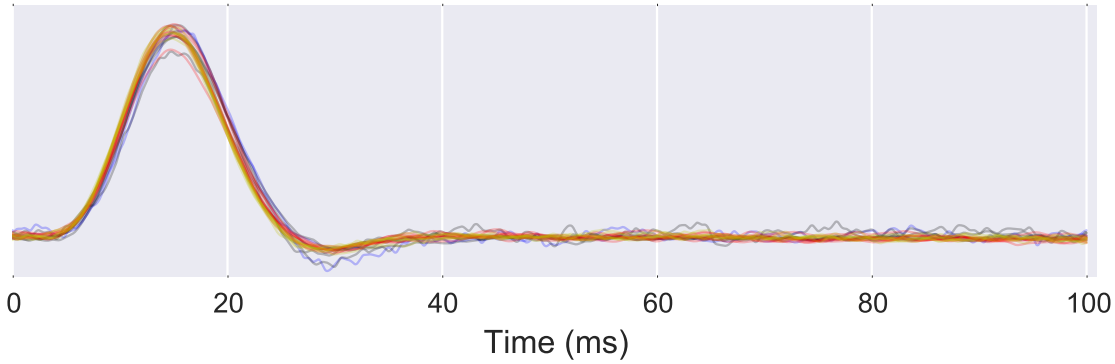

Source: Generated by the author.

Table 8: Time delays found between signals 200 Hz and 27 Hz with DTE. Reference measures for the time delayed transfer entropy calculation.

Experiment ID	Animal Number	DTE (ms) 200 → 27
ID–701	18	15.00
ID–702	18	15.96
ID–766b	22	15.25
ID–773	22	15.25
ID–774	22	14.75
ID–778	22	15.17
ID–781	22	15.00
ID–923	25	15.00
ID–926	25	14.90
ID–929	25	15.10
ID–932	25	14.70
ID–934	25	14.60
ID–937	25	14.70
ID–945	25	14.60
ID–948	25	14.50
ID–1004	26	14.75
ID–1006	26	14.88
ID–1008	26	14.92
ID–1010	26	14.58
ID–1013	26	14.29
ID–1016	26	14.83
ID–1019	26	14.33
Mean		14.76
Standard Deviation		0.25
Normalized Standard Deviation		1.67%

Figure 21: Reference measures for DTE (200 Hz → 58 Hz). The DTE curves shows a peak around the time of 6.50 ms, with a low variation in the measured delay as can be seen in Table 9.

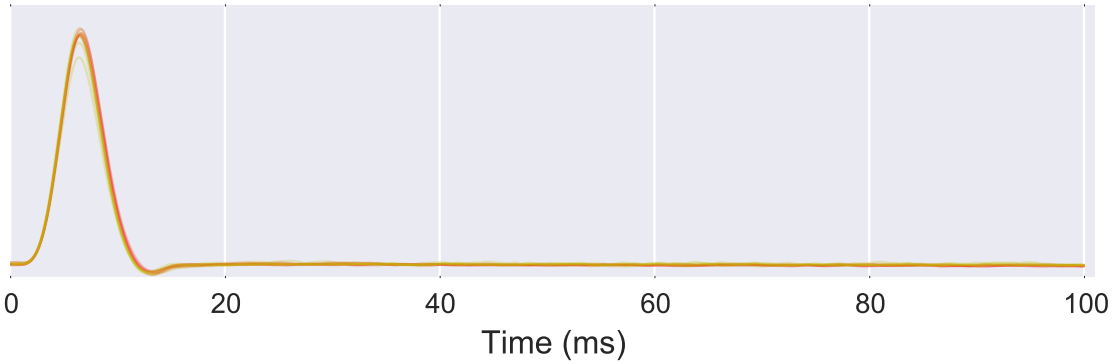

Source: Generated by the author.

Table 9: Time delays found between the signals 200 Hz and 58 Hz using DTE. Reference measures for the time delayed transfer entropy calculation.

Experiment ID	Animal Number	DTE (ms) 200 → 58
ID–765	22	6.79
ID–766a	22	6.67
ID–767	22	6.62
ID–780	22	6.62
ID–924	25	6.60
ID–927	25	6.60
ID–930	25	6.50
ID–935	25	6.50
ID–946	25	6.50
ID–1003	26	7.10
ID–1005	26	6.46
ID–1009	26	6.46
ID–1011	26	6.46
ID–1012	26	7.10
ID–1014	26	6.42
ID–1015	26	7.00
ID–1017	26	6.46
ID–1020	26	6.42
Mean		6.63
Standard Deviation		0.23
Normalized Standard Deviation		3.40%

5.3.2 DTE Between Excitation and SN

It is known that the time delay between two processesis found in the maximum of their DTE (WIBRAL et al., 2013). However, some curves for the DTE $27Hz \rightarrow SN$ (or $58Hz \rightarrow SN$) presented multiple peaks, Figures 22 and 23, and for this reason we divided them in groups with similar characteristics.

DTE 27 Hz → SN

In Table 2 there were 21 experiments performed with the 27 Hz excitation. The interaction 27 Hz → SN was analyzed for each one of these signals, and the curves obtained for their DTE are presented in Figure 22.

The curves of Figure 22 presented variations in their characteristics, such as the value of their time delays and their number of peaks. Twelve curves presented one peak around 17.64 ms, with a normalized standard deviation of 6.86%. Other curves presented two peaks, and the behaviors varied among the samples. The time-delays between excitation and FeCO are presented in Table 10.

Four curves presented a first peak higher than the second. The first peaks were around 7.37 ms with a normalized standard variation of 14.52%, and the second peaks around 23.47 ms with a normalized standard variation of 8.54%.

Three signals presented curves with the first peak smaller than the second. The first peaks were around 7.82 ms with a normalized standard variation of 26.84%, and the second peaks around 23.99 ms with a normalized standard variation of 7.42%.

Other three signals presented two peaks and characteristics similar to the other two cases. However, their peaks were far from the peaks of previous cases, and for this reason, we considered them as outliers.

DTE 58 Hz → SN

In Table 2 there were 15 experiments generated with the 58 Hz excitation. The interaction 58 Hz → SN was analyzed for each one of these signals, and the curves obtained for their DTE are presented in Figure 23.

As in the case of 27 Hz signals, the curves of Figure 23 presented different aspects, such as the time delay and the number of peaks. Nine curves presented one peak around 17.97 ms, with a normalized standard deviation of 4.17%. Other curves presented two peaks, and the behaviors varied among the samples. The time-delays between excitation and SN are presented in Table 11.

Two curves presented a first peak smaller than the second. Their first peaks were around 13.78 ms with a normalized standard variation of 1.85%, and the second peaks were around 21.82 ms with a normalized standard variation of 0.10%.

Figure 22: Delayed transfer entropy between the signals 27 Hz and the SN, testing the connection 27 Hz → SN for the experiments of Table 2. The curves of transfer entropy are presented divided by its characteristics: one peak (A); two peaks when the first is higher than the second (B); two peaks when the second is higher than the first (C); and the outliers (D).

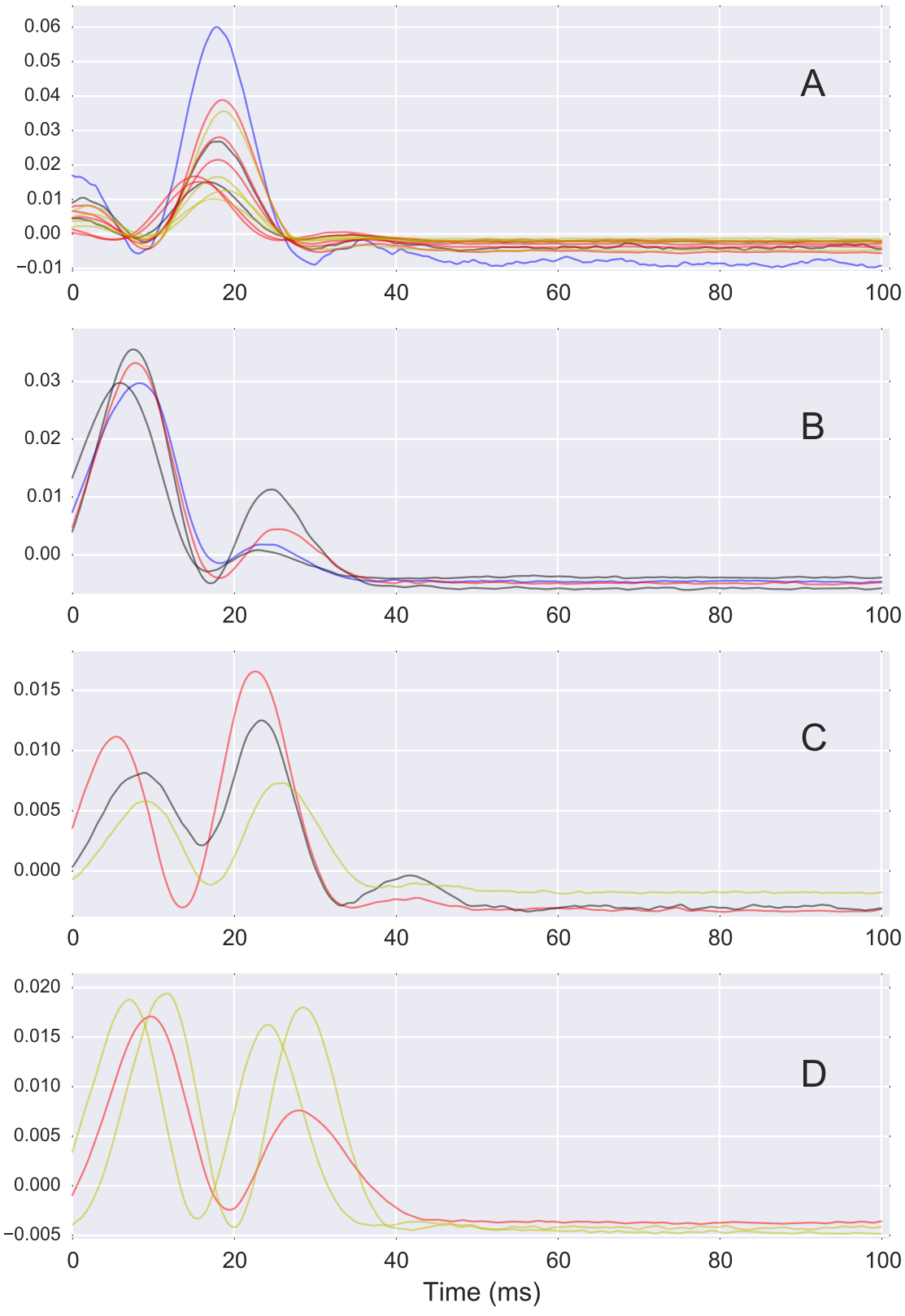

Source: Generated by the author.

Table 10: Time delays between the 27 Hz excitation and SN signals, found with DTE. The samples are divided according to the curves of Figure 22.

Experiment ID	Animal Number	DTE (ms) 27 → SN	
ID–701	18	17.88	
ID–774	22	18.17	
ID–778	22	16.71	
ID–923	25	15.20	
ID–929	25	18.10	
ID–932	25	18.20	
ID–934	25	18.50	
ID–937	25	15.70	
ID–1008	26	17.38	
ID–1010	26	17.88	
ID–1016	26	18.75	
ID–1019	26	19.25	
Mean		17.64	
Standard Deviation		1.21	
Normalized Standard Deviation		6.86%	
ID–702	18	8.29	22.54
ID–781	22	5.83	21.12
ID–766b	22	7.54	24.71
ID–945	25	7.80	25.50
Mean		7.37	23.47
Standard Deviation		1.07	2.00
Normalized Standard Deviation		14.52%	8.54%
ID–773	22	8.88	23.38
ID–926	25	5.4	22.60
ID–1006	26	9.17	26.00
Mean		7.82	23.99
Standard Deviation		2.10	1.78
Normalized Standard Deviation		26.84%	7.42%
Outliers			
ID–948	25	9.70	28.00
ID–1004	26	11.75	28.50
ID–1013	26	7.12	24.21

Figure 23: Delayed transfer entropy between the signals 58 Hz and the SN, testing the connection 58 Hz → SN for the experiments of Table 2. The curves of transfer entropy are presented divided by its characteristics: one peak (A); two peaks when the first is smaller than the second (B); two peaks when the second is smaller than the first (C); and the outliers (D).

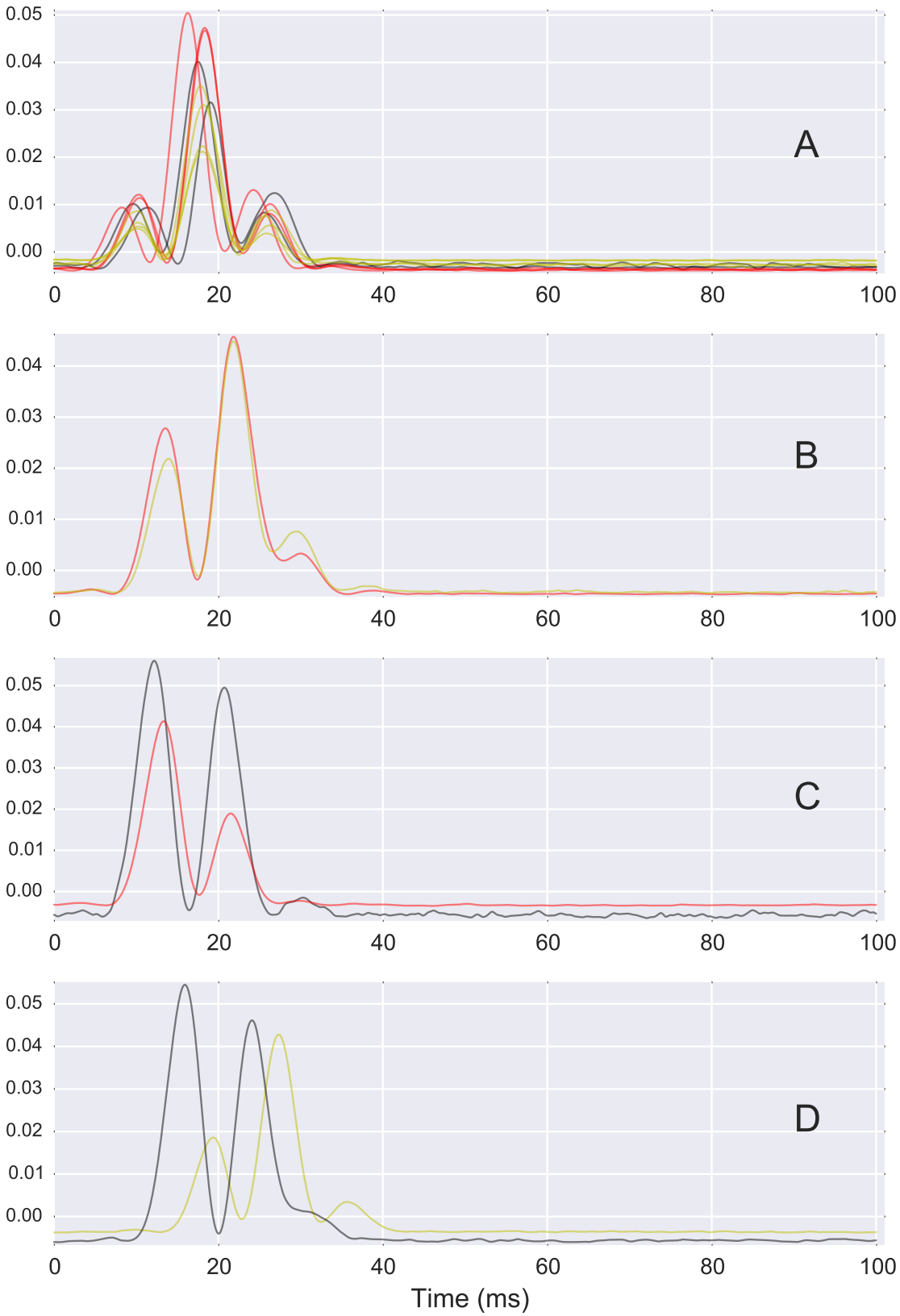

Source: Generated by the author.

Other two signals presented curves with the first peak higher than the second. Their first peaks were around 13.84 ms with a normalized standard variation of 13.68%, and the second peaks were around 22.11 ms with a normalized standard variation of 7.90%.

Another two signals also presented two peaks and characteristics similar to the other two cases. However, their peaks were far from the average of each one of the previous cases, and they were considered as outliers.

Table 11: Time delays between the 58 Hz excitation and SN signals, found with DTE. The samples are divided according to the curves of Figure 23.

Experiment ID	Animal Number	DTE (ms) 58 → SN	
ID–767	22	19.04	
ID–780	22	17.54	
ID–924	25	16.30	
ID–930	25	18.40	
ID–935	25	18.30	
ID–1009	26	18.08	
ID–1011	26	18.17	
ID–1017	26	18.04	
ID–1020	26	17.83	
Mean		17.97	
Standard Deviation		0.75	
Normalized Standard Deviation		4.17%	
ID–927	25	13.60	21.80
ID–1014	26	13.96	21.83
Mean		13.78	21.82
Standard Deviation		0.25	0.02
Normalized Standard Deviation		1.85%	0.10%
ID–765	22	12.21	20.75
ID–946	25	13.40	21.50
Mean		13.84	22.11
Standard Deviation		1.89	1.75
Normalized Standard Deviation		13.68%	7.90%
Outliers			
ID–766a	22	15.92	24.08
ID–1005	26	27.33	33.46

5.4 Groups and Topologies

In the histogram of Figure 17, there were two groups of MTBS separated by a gap, and the histogram of Figure 18 presented three groups. DTE curves presented variations in their forms, and in both cases (27 Hz and 58 Hz) three groups were observed. The lower peaks in some DTE curves with two peaks can be interpreted as the influence of an intermediate node, based on the data processing inequality (see Subsection 3.1.2 and the discussion in Chapter 6). Moreover, the work of Kondoh, Okuma and Newland (1995) also pointed the existence of different spiking rates among the sensory neurons response.

Intending to use our methods of simulation with the locust data, we built the two test cases showed in Figure 24. We put neurons with one peak at DTE curves in one group (G_{1pk}) and the ones with two peaks in another group (G_{2pk}). Topology A from Figure 24 does not present a direct connection between the excitation and the group with two peaks, while topology B does. To find the best model, we performed an *in silico* validation with a simulation of both cases.

Figure 24: Possible topologies for the sensory interaction. Both topologies, a) and b) present the connections $27Hz \rightarrow G_{1pk}$ and $G_{2pk} \rightarrow G_{1pk}$, but only topology b) presents the connection $27Hz \rightarrow G_{2pk}$. These two cases will be simulated to determine the one that better describes the neuronal topology.

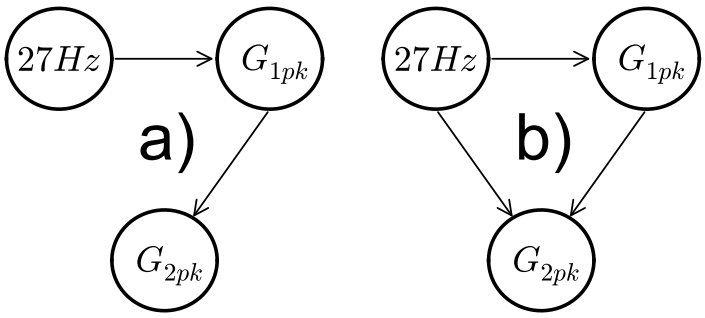

Source: Generated by the author.

5.4.1 Computational Tests and validation

We built four models, one for the 27 Hz signal, another one for SN signals with one peak, and another two for SN signals with two peaks. The samples considered for the 27 Hz model were all the ones presented in Table 10. For the group with one peak, we used all the samples (with one peak) from the same table. The group with two peaks presented an internal divergence, four experiments had the first peak higher than the second, while three others had it smaller. The first model for SN signals with two peaks considered experiments *ID–702*, *ID–781* and *ID–945*, while the second model considered samples *ID–773* and *ID–926*. Experiments *ID-766b* and *ID–1006* were kept for comparisons.

The models were built with the function *histogramdd* from *numpy* (WALT; COLBERT; VAROQUAUX, 2011), which allowed us to assemble probability distributions and joint probability distributions from the data. Since we did not have SN signals recorded simultaneously, it was not possible to use the same methods to calculate the joint probability distribution between the groups of neurons. In this specific point, we used Algorithm 2 to estimate the joint probability distribution.

With the models, we sampled data using the 27 Hz original signal of each sample kept for comparison as the system input. We generated four time series (two for each topology) and compared them with the original time series. A representation of such comparison is presented in Figure 25.

The 27 Hz data entered in the first node and generated some data for the group with one peak. In the sequence, these two sets of data were used to generate data for G_{2pk}. Simulation followed networks topologies and, in case a) only the data G_{1pk} was used in the generation of G_{2pk}, while in case b) G_{1pk} and G_{2pk} were used.

Figure 25: Schematic representation of the SN simulation. The two topologies a) and b) considered in the simulation received the original 27 Hz data, and used it to generate the signals G_{1pk} and G_{2pk}. Both, the original and the synthetic signals, for the group G_{2pk} were segmented into windows (W_{Oi} and W_{Si}) for the analysis.

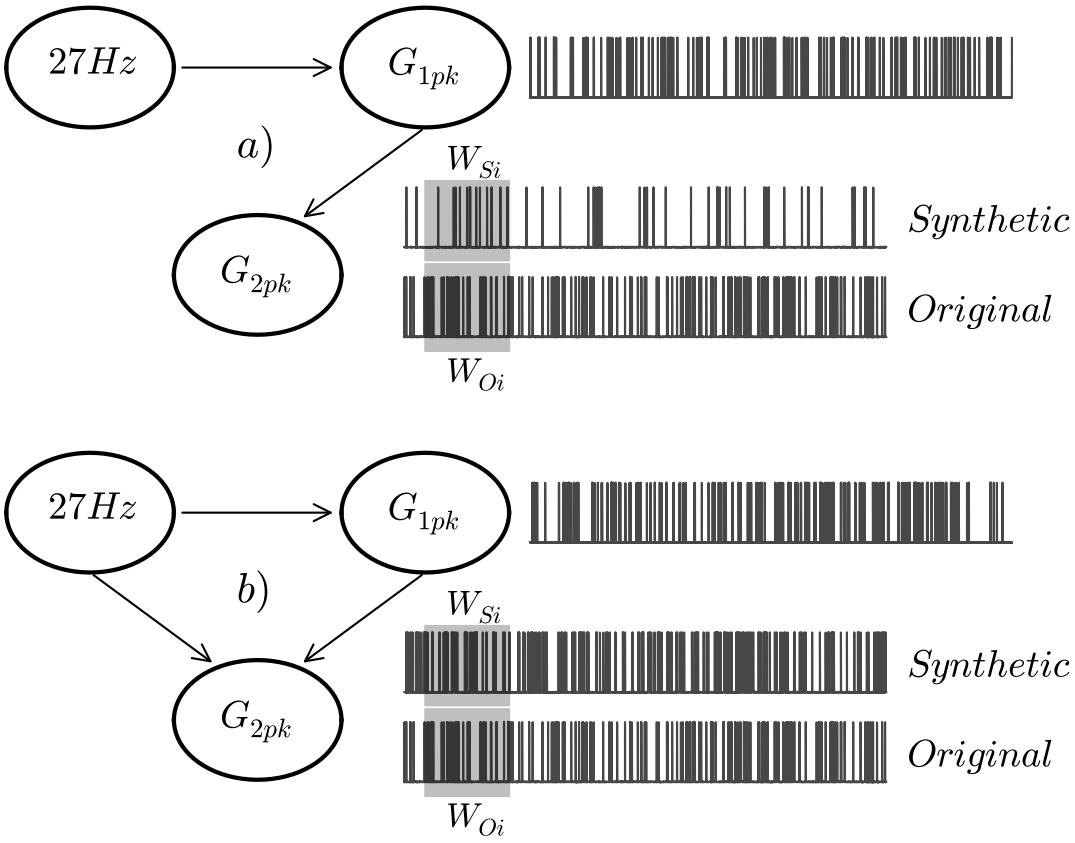

Source: Generated by the author.

The original time series was segmented into 50 windows (W_{Oi}) in such way that each window would present at least 100 spikes. Since both signals (spike actual data and the synthetic one) had the same length, such segmentation was attributed to the simulation data generating another 50 windows (W_{Si}). These procedures allowed us to calculate more MTBS, one for each window W_{Si} and consequently test if the simulated data fitted the original data with the test

$$\begin{cases} H_0: & W_{Si} \in CI\left(W_{Oi}\right) \\ H_1: & W_{Si} \notin CI\left(W_{Oi}\right), \end{cases} \tag{59}$$

where the index i varies from zero to fifth representing each window, and $CI\left(W_{Oi}\right)$ is the confidence interval of the MTBS measured in the respective window.

All tests were compiled and summarized in Table 12, where we show the percentage of synthetic MTBS that fits the original signal. Results show that topology *b)* presented the best fit with 72.00% and 64%, while topology *a)* presented 0% for both. We also added a tolerance of 5% and 10%, and in case of *b)*, both samples increased their fitting, while case *a)* stayed at 0%.

Table 12: Percentage of MTBS from the synthetic data that fit the original MTBS.

Experiment ID	Tolerance 0%	5%	10%
Topology a)			
ID–766b	0.00%	0.00%	0.00%
ID–1006	0.00%	0.00%	0.00%
Topology b)			
ID–766b	72.00%	76.00%	82.00%
ID–1006	64.00%	76.00%	84.00%

5.5 Published Works

5.5.1 9th International Conference on Bio-inspired Systems and Signal Processing, 2016

Modeling of an Insect Proprioceptor System Based on Different Neuron Response Times

Daniel Rodrigues de Lima[1], Michel Bessani[1], Philip Newland[2], and Carlos Dias Maciel[1]
[1]*Department of Electrical and Computational Engineering, University of São Paulo, São Carlos, São Paulo, Brazil*
[2] *Centre for Biological Science, University of Southampton, Highfield Campus, S017 1BJ Southampton, UK*
{*daniel.rodrigues.lima, michel.bessani, carlos.maciel*}*@usp.br, p.l.newland@soton.ac.uk*

Keywords: Neuronal Spike Signals; Neuronal Response; Desert Locust; FeCO; Transfer Entropy; Inter-Spike Interval; Survival Analysis.

Abstract: This paper analyzes neuronal spiking signals from the Desert Locust Femorotibial Chordotonal Organ (FeCO). The data comes from records of the insect neuronal response due to external stimulation. We measured the Inter-Spike Interval (ISI) and calculated Transfer Entropy for investigate different FeCO responses. ISI is a technique that measures the time between two spikes; and transfer entropy is a theoretical information measure used to find dependencies and causal relationships. We also use survival functions to assemble FeCO models. Furthermore, this work uses and compares results of two approaches, one with transfer entropy and other with ISI measures. The results indicate evidence to support the existence of more than one type of FeCO neuron.

5.5.2 7th International Conference on Bioinformatics Models, Methods and Algorithms, 2016

Synthetic Data Generation Based on Mutual Information and Surrogate Data for Bayesian Network Models

Daniel Rodrigues de Lima and Carlos Dias Maciel
[1]*Department of Electrical Engineering and Computing, University of São Paulo, Avenida Trabalhador São-Carlense 400, São Carlos, São Paulo, Brazil*
{*daniel.rodrigues.lima, carlos.maciel*}*@usp.br*

Keywords: Bayesian Network; Mutual Information; Surrogate Time Series; Synthetic Data.

Abstract: Bayesian Networks (BNs) are Direct Acyclic Graphs, a set of edges and nodes that represents a Joint Probability Distribution (JPD). The BN technique is widely used in Bioinspired Engineering and Bioinformatics as a machine-learning tool to analyze biological datasets, assemble models from biological structures, and study biological process. In this work, we present a method to simulate BNs. Our methodology is based in an Information Theoretic measure, the Mutual Information (MI), which allows the detection of independences between random variables. Additionally, we use Surrogate Time Series to establish a threshold for MI measures. Above that threshold, all MI levels are considered as dependencies. This threshold will improve the synthetic data generated from the noise influence. As an application, motivation, and suggestion for future works, we also present the simulation of a small neuronal insect network.

5.5.3 CBA2016 - XXI Congresso Brasileiro de Automática, 2016

NETWORK STRUCTURAL RECONSTRUCTION BASED ON DELAYED TRANSFER ENTROPY AND SYNTHETIC DATA

Daniel Rodrigues de Lima*, Fernando Pasquini Santos*, Carlos Dias Maciel*

*Department of Electrical and Computational Engineering
University of São Paulo
São Carlos, São Paulo, Brazil

Email: {daniel.rodrigues.lima;fernando.pasquini.santos;carlos.maciel}@usp.br

Abstract— The knowledge of how signals are received, processed, and transmitted in neuronal systems is one of the bio-inspired engineering objectives. In this area, not only the physiology of separated neurons is relevant, but also, the connections among them, the neuronal topology. A modeling process of such biological system requires the integration of both, physiological and topological properties. However, there is a limitation in the modeling process due to the impossibility of recording the activity of all the system neurons at the same time. To solve this problem, we propose the usage of simulations and information theoretic measures to infer a network topology. Three test cases were simulated, and the interactions were measured with Transfer Entropy resulting in topology candidates. In two cases we could visually recover the connections from the graphs. In a third case we found a residual connection which allowed us to explore some properties from the network topology.

Keywords— Bio-inspired engineering; neuronal systems; simulation; information theoretic measures; network topology.

Resumo— Compreender o funcionamento dos processos de recepção, processamento e transmissão de informação nos sistemas neuronais é um dos objetivos da engenharia bio-inspirada. Nesse campo de estudo, não somente a fisiologia neuronal é relevante, mas também faz-se necessário o conhecimento sobre a organização da topologia dos neurônios. A modelagem desses sistemas requer a integração de aspectos fisiológicos e topológicos. No entanto, existem limites no processo de modelagem devido à impossibilidade de gravar a atividade de todos os neurônios simultaneamente. Para resolver este problema, propõe-se o uso de simulações e medidas de teoria da informação para inferir uma topologia de redes. Simulou-se três casos de teste e as interações entre variáveis foram medidas com Transferência de Entropia. Em dois casos foi possível recuperar as conexões apenas observando os resultados gráficos. Em um terceiro caso, encontrou-se uma conexão residual, a qual permitiu que algumas propriedades da topologia de rede fossem exploradas.

Palavras-chave— Engenharia bio-inspirada; sistemas neuronais; simulações; medidas de teoria da informação; topologia de rede.

Chapter 6

Discussion and Conclusions

In this study, we analyzed and modeled the response of sensory neurons due to FeCO stimulation with Gaussian white noise. We looked into electrophysiological recordings observing their spiking rates and information shares. Signals were collected in a previous study (KONDOH; OKUMA; NEWLAND, 1995) that examined the sensibility of sensory neurons to position, velocity, and acceleration, and also pointed the existence of different spiking rates among the neuronal signals.

Based on the priori information about differences among spiking rates, we started our analysis confirming it with the metric mean time between spikes. In the sequence, we tested the existence of connections between excitation and sensory neurons with the help of DTE. The curves $time \times DTE$ allowed us to separate experiments in groups with similar characteristics (one peak, two peaks with the first smaller than the second, among others.).

We also developed a method to estimate joint probability distributions, which was used in Section 5.4. However, our algorithms still need to be more tested and explored, either by stressing their limits or applying them in different scenarios. In this chapter, we will discuss our results, and point the next steps of our research.

Algorithms Validation

DTE allowed the reconstruction of connections $GWN \rightarrow Spk1$ and $Spk1 \rightarrow Spk2$, for the three cases proposed in Figure 13. Both properties, the time delay and the direction of information flow, were found in the dataset when measuring DTE. Results matched the expected values of time delay presented in Table 3, and also found the expected connections, shown in Figure 13.

Connection $GWN \rightarrow Spk2$ was found for all three cases, but it was expected to be found only in two of them. The existence of such connection in cases B and C was expected, however, case A does not present it and Figure 15 should not suggest the existence of such connection.

The difference between the peak of the case A and the ground noise of DTE is lower than the one presented by the other graphs, as can be seen in Figures 14, 15, and 16. The peak for $GWN \rightarrow Spk2$ in case A is only 0.84% higher than its respective ground noise, while in all other cases such difference is 5.48% and 10.00%. The percentage differences of peak values and the correspondent maximum of the ground noise is summarized in Table 4.

DTE, as presented by Wibral, Vicente and Lindner (2014), is the delayed mutual information of two processes, given the past of one of them. Thus it is subjected to mutual information properties, including the data processing inequality. Data processing inequality (COVER; THOMAS, 2006) is an information theoretical property which states that the existence of an intermediary variable between two processes will reduce the mutual information of them.

In case A, the peak of information transfer for $GWN \rightarrow Spk1$ was 17.3% higher than its respective ground noise. In the same case, the peak found in connection $Spk1 \rightarrow Spk2$ was 14.62% higher than its ground noise. Still in the same case, the peak for connection $GWN \rightarrow Spk2$ was only 0.84% higher than its ground noise. Based on the data processing inequality and considering topology A from Figure 13, we see that there is an indirect connection between $GWN \rightarrow Spk2$, i.e., there is an intermediate node ($Spk1$) between them. Therefore, based on the data processing inequality, it can be assumed that the low peak presented in Figure 15 is due to this indirect connection.

Different Spiking Rates

When Kondoh, Okuma and Newland (1995) analyzed the neuronal responses due to the 27 Hz excitation or 58 Hz, they observed different spiking rates. MTBS was used to show that sensory neurons present different responses for both excitations, which can be seen in the histograms of Figures 17 and 18, in Tables 5 and 6, and also in the curves of Figures 19.

In the case of the survival function models, we can see that the confidence intervals ($\alpha = 5\%$) are non-overlapping for 27 Hz signals (it was not possible to do the same models for all groups of 58 Hz experiments since there was not sufficient data). Such property allows us to state with 95% of certainty (in the case of 27 Hz experiments) that they represent different neuronal responses.

Although we have found evidence to support the assumption of different spiking rates, we cannot state that there are two groups (or three as suggested by 58 Hz experiments). The reason is that we do not have sufficient data to perform statistical validations (12 and 6 samples for groups in 27 Hz experiments, and 14, 2, and 2 samples in the 58 Hz). However, we can say that there is evidence that the neuronal response to the same excitation is not the same in all sensory neurons, and that further experiments should be done.

Interactions Between Groups of Neurons

As defined by Wibral, Vicente and Lindner (2014), DTE is the information shared between two variables, given the past of the variable of interest (see Equation 28). In such calculations, memory effects of the target variable are disregarded, and a peak in DTE indicates the existence of a connection between those variables. As a result, a peak is not an effect of the variable's past. Consequently, when the DTE calculated between excitation and sensory neurons presents two peaks, it leads us to consider the possibility that sensory neurons are influenced twice by the excitation, i.e., they process the position signal $x(t)$ and its past $x(t-\tau)$, where τ is a time-delay.

In the algorithms validation, the definition of DTE as a delayed mutual information has led us to see that it follows the data processing inequality (COVER; THOMAS, 2006). In the same way, small peaks in DTE curves leads us to assume that they are the result of indirect influences of the excitation in sensory neurons. However, to make such assumptions, we have to consider the existence of intermediate layers responsible for the peaks with low amplitudes.

Hypothesis

Besides the existence of different spiking rates among sensory neurons, Kondoh, Okuma and Newland (1995) showed that they were sensitive to position, velocity and acceleration. They pointed that neurons with low spiking rates (high MTBS) should respond to acceleration, position sensitive neurons would present high spiking rates (low MTBS), and neurons sensitive to velocity would present an intermediate spiking rate. The reason for those assumptions is that velocity is coded only when the position is changed, and acceleration is coded only when velocity changes (KONDOH; OKUMA; NEWLAND, 1995).

Three curves from Figure 22-B are from the group of experiments that presented MTBS with low spiking rates (ID–702, ID–766b, ID–781), and one is from the group with low MTBS (ID–945). However, the MTBS of experiment ID–945 was 32.63 ms, which is 36% higher than the group mean, and outside the group confidence interval (Tables 5 and 7). We could assume that these signals are responses to acceleration because of their high MTBS, and we could also assume that experiments in graphic C of Figure 22 are due to velocity, since they present intermediate MTBS. However, in both cases we cannot state with our analysis which signal is the neuronal response to position, velocity, or acceleration. What we can affirm here (based on DTE analysis) is that if the same kind of neurons codifies different Physical quantities, then there should be preprocessing layers, such as suggested in Figure 26.

Figure 26: Model for the insect proprioceptor system with a preprocessing layer. This diagram includes an intermediate layer, which is responsible for preprocessing the signal $x(t)$, generating $v(t)$ and $a(t)$ that will be codified into spiking signals by the sensory neurons.

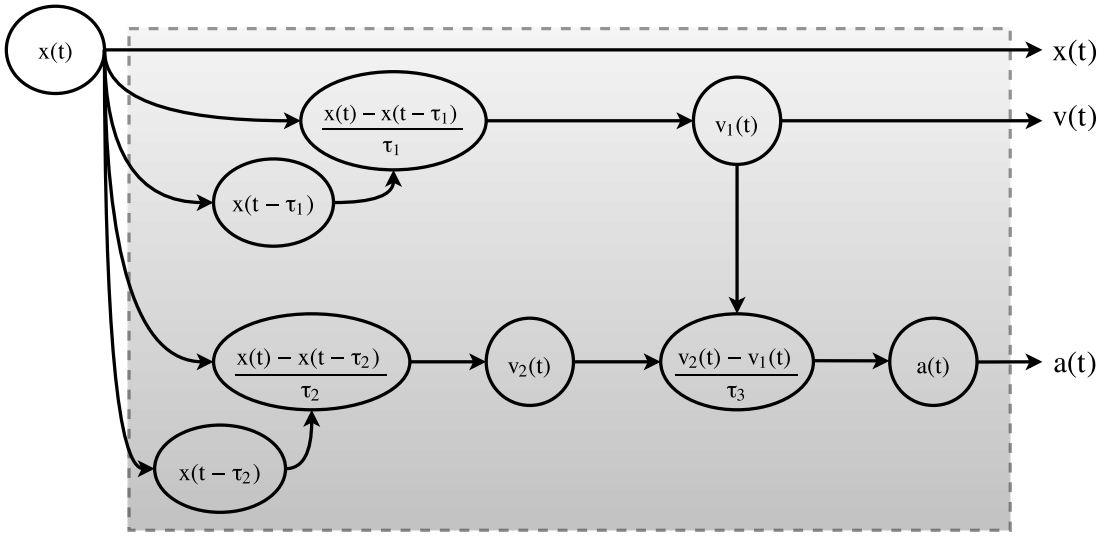

Source: Generated by the author.

Next Steps

The system of Figure 26 is a mere speculation of the neuronal circuit internal organization, what we know at this time is that there are evidence of an intermediate layer. For example, supposing that the neuronal system is similar to Figure's 26 diagram, then there are time-delayer nodes that allows the comparison of the current position $x(t)$ with its past $x(t-\tau_1)$ in order to calculate the locust hind leg velocity $v(t)$, i.e., it performs the operation

$$v_1(t) = \frac{d}{dt}x(t) \approx \frac{x(t) - x(t-\tau_1)}{\tau_1}, \tag{60}$$

where $x(t)$ is the 27 Hz signal, and τ_1 is a time delay. In the same way, the acceleration would be determined by the comparison of two values of velocity, i.e., the operation

$$a(t) = \frac{d}{dt}v(t) \approx \frac{v_2(t) - v_1(t)}{\tau_3}, \tag{61}$$

where $v_1(t)$ comes from the velocity sensitive layer.

The assumption of intermediate nodes, i.e., a preprocessing layer opens many possibilities for further investigations. Firstly, it has to be confirmed that some neurons respond to velocity and acceleration, and this can be done with DTE. If a neuron responds to velocity, DTE results should be as follows

$$\begin{cases} DTE\left(\frac{d}{dt}x(t) \to SN\right) > DTE\left(x(t) \to SN\right) \\ DTE\left(\frac{d}{dt}x(t) \to SN\right) > DTE\left(\frac{d^2}{dt^2}x(t) \to SN\right), \end{cases} \tag{62}$$

In the same way, if a neuron responds to acceleration, then

$$\begin{cases} DTE\left(\frac{d^2}{dt^2}x(t) \to SN\right) > DTE\left(x(t) \to SN\right) \\ DTE\left(\frac{d^2}{dt^2}x(t) \to SN\right) > DTE\left(\frac{d}{dt}x(t) \to SN\right). \end{cases} \tag{63}$$

And for a position sensitive neuron, DTE results should be

$$\begin{cases} DTE\left(x(t) \to SN\right) > DTE\left(\frac{d}{dt}x(t) \to SN\right) \\ DTE\left(x(t) \to SN\right) > DTE\left(\frac{d^2}{dt^2}x(t) \to SN\right). \end{cases} \tag{64}$$

If confirmed that some sensory neurons are codifying position, while others velocity, and others acceleration, it is necessary to investigate if there is any information share between the different neurons, and at this point, we think that our algorithms will be able to contribute. Next steps of our work include analyzing the response of neurons to position, velocity and acceleration with DTE; determining whether or not the preprocessing layer exists, and if positive (as expected to be) future studies will be required to investigate its internal structure.

Bibliography

ACHCAR, J. A.; MOALA, F. A. Use of copula functions for the reliability of series systems. **International Journal of Quality & Reliability Management**, 2015. Emerald Group Publishing Limited, v. 32, n. 6, p. 617–634, 2015.

ALONSO, J. F. et al. Evaluation of respiratory muscles activity by means of cross mutual information function at different levels of ventilatory effort. **IEEE Transactions on Biomedical Engineering**, 2007. IEEE, v. 54, n. 9, p. 1573–1582, 2007.

BAR-COHEN, Y. Biomimetics – using nature to inspire human innovation. **Bioinspiration & biomimetics**, 2006. IOP Publishing, v. 1, n. 1, p. P1, 2006.

BARNETT, L.; BARRETT, A. B.; SETH, A. K. Granger causality and transfer entropy are equivalent for gaussian variables. **Physical review letters**, 2009. APS, v. 103, n. 23, p. 238701, 2009.

BAUER, M. et al. Finding the direction of disturbance propagation in a chemical process using transfer entropy. **Control Systems Technology, IEEE Transactions on**, 2007. IEEE, v. 15, n. 1, p. 12–21, 2007.

BEWICK, V.; CHEEK, L.; BALL, J. Statistics review 12: survival analysis. **CRITICAL CARE-LONDON-**, 2004. v. 8, p. 389–394, 2004.

BHARADWAJ, R.; BANERJEE, S. The nervous system of the desert locust, schistocerca gregaria (orthoptera: Acrididae) with a discussion on muscle innervation. **Journal of Natural History**, 1971. Taylor & Francis, v. 5, n. 2, p. 183–208, 1971.

BROWN, E. N.; KASS, R. E.; MITRA, P. P. Multiple neural spike train data analysis: state-of-the-art and future challenges. **Nat Neurosci**, 2004. v. 7, n. 5, p. 456–461, maio 2004.

BURROWS, M. Parallel processing of proprioceptive signals by spiking local interneurons and motor neurons in the locust. **The Journal of neuroscience**, 1987. Soc Neuroscience, v. 7, n. 4, p. 1064–1080, 1987.

BURROWS, M. **The neurobiology of an insect brain**. [S.l.]: Oxford University Press Oxford, 1996.

BUSCHMANN, T. et al. Controlling legs for locomotion–insights from robotics and neurobiology. **Bioinspiration & biomimetics**, 2015. IOP Publishing, v. 10, n. 4, p. 041001, 2015.

CABRERO, M. et al. Discontinuation of hypomethylating agent therapy in patients with myelodysplastic syndromes or acute myelogenous leukemia in complete remission or partial response: Retrospective analysis of survival after long-term follow-up. **Leukemia Research**, 2015. v. 39, n. 5, p. 520 – 524, 2015. ISSN 0145-2126. Disponível em: <http://www.sciencedirect.com/science/article/pii/S0145212615000752>.

CARDINALI, L. et al. Proprioception is necessary for body schema plasticity: Evidence from a deafferented patient. **Frontiers in Human Neuroscience**, 2016. Frontiers Media SA, v. 10, 2016.

CHEN, L. et al. Detection of bursts in neuronal spike trains by the mean inter-spike interval method. **Progress in Natural Science**, 2009. v. 19, n. 2, p. 229 – 235, 2009. ISSN 1002-0071. Disponível em: <http://www.sciencedirect.com/science/article/pii-/S1002007108003432>.

COLLETT, D. **Modelling survival data in medical research**. London, New York: Chapman & Hall, 2003. (Texts in statistical science). ISBN 1-58488-325-1. Disponível em: <http://opac.inria.fr/record=b1135017>.

COLOMBO, R. et al. Improving proprioceptive deficits after stroke through robot-assisted training of the upper limb: a pilot case report study. **Neurocase**, 2016. v. 22, n. 2, p. 191–200, 2016. PMID: 26565132. Disponível em: <http://dx.doi.org/10.1080-/13554794.2015.1109667>.

COVER, T. M.; THOMAS, J. A. Elements of information theory 2nd edition. 2006. Wiley–interscience, 2006.

CUPPONE, A. et al. Proprioceptive assessment of the wrist joint across both joint degrees of freedom. In: **2015 IEEE International Conference on Rehabilitation Robotics (ICORR)**. [S.l.: s.n.], 2015. p. 894–898. ISSN 1945-7898.

DEMARIE-DREBLOW, D. Relation between knowledge and memory: A reminder that correlation does not imply causality. **Child Development**, 1991. Wiley Online Library, v. 62, n. 3, p. 484–498, 1991.

DEWHIRST, O. Nonlinear system analysis of local reflex control of locust hind limbs. October 2012. Disponível em: <http://eprints.soton.ac.uk/351342/>.

DEWHIRST, O. P. et al. The dynamics of locust non-spiking local interneurons. In: **BIOSIGNALS 2011. Proceedings of the International Conference on Bio-inspired Systems and Signal Processing, Rome, Italy**. [S.l.: s.n.], 2011. p. 26–29.

DEWHIRST, O. P. et al. A system identification analysis of neural adaptation dynamics and nonlinear responses in the local reflex control of locust hind limbs. **Journal of computational neuroscience**, 2013. Springer, v. 34, n. 1, p. 39–58, 2013.

DEWHIRST et al. Neuromuscular reflex control of limb movement-validating models of the locusts hind leg control system using physiological input signals. In: IEEE. **Neural Engineering, 2009. NER'09. 4th International IEEE/EMBS Conference on**. [S.l.], 2009. p. 689–692.

DINCER, I.; CENGEL, Y. A. Energy, entropy and exergy concepts and their roles in thermal engineering. **Entropy**, 2001. v. 3, n. 3, p. 116, 2001. ISSN 1099-4300. Disponível em: <http://www.mdpi.com/1099-4300/3/3/116>.

DOLAN, K. T.; SPANO, M. L. Surrogate for nonlinear time series analysis. **Phys. Rev. E**, 2001. American Physical Society, v. 64, p. 046128, Sep 2001. Disponível em: <http://link.aps.org/doi/10.1103/PhysRevE.64.046128>.

ENDO, W. Modelagem de circuitos neurais do sistema neuromotor e proprioceptor de insetos com o uso da transferência de informação entre conexões neurais. March 2014. Disponível em: <http://www.teses.usp.br/teses/disponiveis/18/18153/tde-06052014-163332/en.php>.

ENDO, W. et al. Delayed mutual information infers patterns of synaptic connectivity in a proprioceptive neural network. **Journal of computational neuroscience**, 2015. Springer, v. 38, n. 2, p. 427–438, 2015.

GOLDBERGER, J.; GORDON, S.; GREENSPAN, H. An efficient image similarity measure based on approximations of kl-divergence between two gaussian mixtures. In: IEEE. **Computer Vision, 2003. Proceedings. Ninth IEEE International Conference on**. [S.l.], 2003. p. 487–493.

HARRELL, F. E. **Regression modeling strategies: with applications to linear models, logistic regression, and survival analysis**. [S.l.]: Springer Science & Business Media, 2013.

HILLIER, S.; IMMINK, M.; THEWLIS, D. Assessing proprioception: A systematic review of possibilities. **Neurorehabilitation and Neural Repair**, 2015. v. 29, n. 10, p. 933–949, 2015. Disponível em: <http://nnr.sagepub.com/content/29/10/933.abstract>.

HUGHES, C. M. L. et al. Upper extremity proprioception in healthy aging and stroke populations, and the effects of therapist- and robot-based rehabilitation therapies on proprioceptive function. **Frontiers in Human Neuroscience**, 2015. v. 9, p. 120, 2015. ISSN 1662-5161. Disponível em: <http://journal.frontiersin.org/article/10.3389/fnhum-.2015.00120>.

JIN, S.-H.; LIN, P.; HALLETT, M. Linear and nonlinear information flow based on time-delayed mutual information method and its application to corticomuscular interaction. **Clinical Neurophysiology**, 2010. v. 121, n. 3, p. 392 – 401, 2010. ISSN 1388-2457. Disponível em: <http://www.sciencedirect.com/science/article/pii-/S1388245709006671>.

KANTZ, H.; SCHREIBER, T. **Nonlinear time series analysis**. [S.l.]: Cambridge university press, 2004.

KLEIN, J. P.; MOESCHBERGER, M. L. **Survival analysis: techniques for censored and truncated data**. [S.l.]: Springer Science & Business Media, 2003.

KONDOH, Y.; OKUMA, J.; NEWLAND, P. L. Dynamics of neurons controlling movements of a locust hind leg: Wiener kernel analysis of the responses of proprioceptive afferents. **Journal of Neurophysiology**, 1995. American Physiological Society, v. 73, n. 5, p. 1829–1842, 1995. ISSN 0022-3077. Disponível em: <http://jn.physiology.org-/content/73/5/1829>.

KULLBACK, S.; LEIBLER, R. A. On information and sufficiency. **The annals of mathematical statistics**, 1951. JSTOR, v. 22, n. 1, p. 79–86, 1951.

LAWLESS, J. F. **Statistical models and methods for lifetime data**. [S.l.]: John Wiley & Sons, 2011.

LEGENDY, C.; SALCMAN, M. Bursts and recurrences of bursts in the spike trains of spontaneously active striate cortex neurons. **Journal of neurophysiology**, 1985. Am Physiological Soc, v. 53, n. 4, p. 926–939, 1985.

LI, W. et al. **Reliability Assessment of Electrical Power Systems Using Monte Carlo Methods**. [S.l.]: Springer Science & Business Media, 1994.

LINDLEY, D. **Boltzmann's atom: the great debate that launched a revolution in physics**. [S.l.]: Simon and Schuster, 2001.

MACIEL, C. D.; SIMPSON, D. M.; NEWLAND, P. L. Inference about multiple pathways in motor control limb in locust. In: **BIOSIGNALS**. [S.l.: s.n.], 2012. p. 69–75.

MACKENZIE, T. et al. Longevity of patients with cystic fibrosis in 2000 to 2010 and beyond: survival analysis of the cystic fibrosis foundation patient registry. **Annals of internal medicine**, 2014. Am Coll Physicians, v. 161, n. 4, p. 233–241, 2014.

MANAL, K.; ROSE, W. A general solution for the time delay introduced by a low-pass butterworth digital filter: An application to musculoskeletal modeling. **Journal of biomechanics**, 2007. Elsevier, v. 40, n. 3, p. 678–681, 2007.

MCDONNELL, M. D.; IKEDA, S.; MANTON, J. H. An introductory review of information theory in the context of computational neuroscience. **Biological cybernetics**, 2011. Springer, v. 105, n. 1, p. 55–70, 2011.

MERUELO, A. C. et al. Improved system identification using artificial neural networks and analysis of individual differences in responses of an identified neuron. **Neural Networks**, 2016. Elsevier, v. 75, p. 56–65, 2016.

MILLMAN, K. J.; AIVAZIS, M. Python for scientists and engineers. **Computing in Science Engineering**, 2011. v. 13, n. 2, p. 9–12, March 2011. ISSN 1521-9615.

NEWLAND, P. L.; KONDOH, Y. Dynamics of neurons controlling movements of a locust hind leg iii. extensor tibiae motor neurons. **Journal of Neurophysiology**, 1997. American Physiological Society, v. 77, n. 6, p. 3297–3310, 1997. ISSN 0022-3077. Disponível em: <http://jn.physiology.org/content/77/6/3297>.

NICHOLS, J. Examining structural dynamics using information flow. **Probabilistic Engineering Mechanics**, 2006. Elsevier, v. 21, n. 4, p. 420–433, 2006.

OLIPHANT, T. E. Python for scientific computing. **Computing in Science Engineering**, 2007. v. 9, n. 3, p. 10–20, May 2007. ISSN 1521-9615.

PAPANA, A.; KUGIUMTZIS, D.; KYRTSOU, C. A nonparametric causality test: Detection of direct causal effects in multivariate systems using corrected partial transfer entropy. In: **Topics in Nonparametric Statistics**. [S.l.]: Springer, 2014. p. 197–206.

PEARL, J. Causal diagrams for empirical research. **Biometrika**, 1995. v. 82, n. 4, p. 669–688, 1995. Disponível em: <http://biomet.oxfordjournals.org/content/82/4/669-.abstract>.

PEEBLES, P. Z.; READ, J.; READ, P. **Probability, random variables, and random signal principles**. [S.l.]: McGraw-Hill Boston, Mass, USA, 2001.

PFLÜGER, H.-J.; DUCH, C. Dynamic neural control of insect muscle metabolism related to motor behavior. **Physiology**, 2011. American Physiological Society, v. 26, n. 4, p. 293–303, 2011. ISSN 1548-9213. Disponível em: <http://physiologyonline-.physiology.org/content/26/4/293>.

RAJANNA, R.; CAO, L.; VISWANATHAN, R. Divergence and bayes error based soft decision for decentralized signal detection of correlated sensor data. In: IEEE. **2016 Annual Conference on Information Science and Systems (CISS)**. [S.l.], 2016. p. 490–495.

REICH, D. S. et al. Interspike intervals, receptive fields, and information encoding in primary visual cortex. **The Journal of Neuroscience**, 2000. v. 20, n. 5, p. 1964–1974, 2000. Disponível em: <http://www.jneurosci.org/content/20/5/1964.abstract>.

REINSTEIN, M.; HOFFMANN, M. Dead reckoning in a dynamic quadruped robot based on multimodal proprioceptive sensory information. **IEEE Transactions on Robotics**, 2013. v. 29, n. 2, p. 563–571, April 2013. ISSN 1552-3098.

RITZMANN, R. E.; BÜSCHGES, A. 10 insect walking: From reduced preparations to natural terrain. **Cold Spring Harbor Monograph Archive**, 2007. v. 49, p. 229–250, 2007.

ROCHA, J. de la et al. Correlation between neural spike trains increases with firing rate. **Nature**, 2007. Nature Publishing Group, v. 448, n. 7155, p. 802–806, ago. 2007. ISSN 1476-4687. Disponível em: <http://dx.doi.org/10.1038/nature06028>.

RUSSELL, S. J. et al. **Artificial intelligence: a modern approach**. [S.l.]: Prentice hall Upper Saddle River, 2003.

SARLEGNA, F. R. et al. Force-field adaptation without proprioception: Can vision be used to model limb dynamics? **Neuropsychologia**, 2010. v. 48, n. 1, p. 60 – 67, 2010. ISSN 0028-3932. Disponível em: <http://www.sciencedirect.com/science/article/pii-/S0028393209003285>.

SCHREIBER, T. Measuring information transfer. **Physical review letters**, 2000. APS, v. 85, n. 2, p. 461, 2000.

SCHREIBER, T.; SCHMITZ, A. Surrogate time series. **Physica D: Nonlinear Phenomena**, 2000. Elsevier, v. 142, n. 3, p. 346–382, 2000.

SCHWALGER, T.; DROSTE, F.; LINDNER, B. Statistical structure of neural spiking under non-poissonian or other non-white stimulation. **Journal of Computational Neuroscience**, 2015. Springer US, v. 39, n. 1, p. 29–51, 2015. ISSN 0929-5313. Disponível em: <http://dx.doi.org/10.1007/s10827-015-0560-x>.

SILCHENKO, A. N. et al. Data-driven approach to the estimation of connectivity and time delays in the coupling of interacting neuronal subsystems. **Journal of neuroscience methods**, 2010. Elsevier, v. 191, n. 1, p. 32–44, 2010.

SORIANO, M. C. et al. Synchronization in simple network motifs with negligible correlation and mutual information measures. **Physical review letters**, 2012. APS, v. 108, n. 13, p. 134101, 2012.

VENEMA, V.; AMENT, F.; SIMMER, C. A stochastic iterative amplitude adjusted fourier transform algorithm with improved accuracy. **Nonlinear Processes in Geophysics**, 2006. Copernicus GmbH, v. 13, n. 3, p. 321–328, 2006.

VICENTE, R. et al. Transfer entropy–a model-free measure of effective connectivity for the neurosciences. **Journal of computational neuroscience**, 2011. Springer, v. 30, n. 1, p. 45–67, 2011.

VIDAL-GADEA, A. G. et al. Coding characteristics of spiking local interneurons during imposed limb movements in the locust. **Journal of neurophysiology**, 2010. Am Physiological Soc, v. 103, n. 2, p. 603–615, 2010.

WALPOLE, R. et al. **Probability and Statistics for Engineers and Scientists**. [S.l.]: Prentice Hall 9. Course Policies, 2014.

WALT, S. van der; COLBERT, S. C.; VAROQUAUX, G. The numpy array: A structure for efficient numerical computation. **Computing in Science Engineering**, 2011. v. 13, n. 2, p. 22–30, March 2011. ISSN 1521-9615.

WESSNITZER, J.; WEBB, B. Multimodal sensory integration in insects–towards insect brain control architectures. **Bioinspiration & biomimetics**, 2006. IOP Publishing, v. 1, n. 3, p. 63, 2006.

WIBRAL, M. et al. Measuring information-transfer delays. **PloS one**, 2013. Public Library of Science, v. 8, n. 2, p. e55809, 2013.

WIBRAL, M.; VICENTE, R.; LINDNER, M. Transfer entropy in neuroscience. In: **Directed Information Measures in Neuroscience**. [S.l.]: Springer, 2014. p. 3–36.

YANG, C. et al. Detecting information flow direction in multivariate linear and nonlinear models. **Signal Processing**, 2013. v. 93, n. 1, p. 304 – 312, 2013. ISSN 0165-1684. Disponível em: <http://www.sciencedirect.com/science/article/pii-/S0165168412001636>.

YANG, F.; XIAO, D. Progress in root cause and fault propagation analysis of large-scale industrial processes. **Journal of Control Science and Engineering**, 2012. Hindawi Publishing Corporation, v. 2012, 2012.

YU, D. et al. Kl-divergence regularized deep neural network adaptation for improved large vocabulary speech recognition. In: IEEE. **Acoustics, Speech and Signal Processing (ICASSP), 2013 IEEE International Conference on**. [S.l.], 2013. p. 7893–7897.

ZHANG, Q. et al. Bioinspired engineering of honeycomb structure–using nature to inspire human innovation. **Progress in Materials Science**, 2015. Elsevier, v. 74, p. 332–400, 2015.

ZHOU, Z. et al. A proprioceptive neuromuscular facilitation integrated robotic ankle–foot system for post stroke rehabilitation. **Robotics and Autonomous Systems**, 2015. v. 73, p. 111 – 122, 2015. ISSN 0921-8890. Wearable Robotics. Disponível em: <http://www.sciencedirect.com/science/article/pii/S0921889014002085>.

ZIO, E. **The Monte Carlo simulation method for system reliability and risk analysis**. [S.l.]: Springer, 2013.

Attachments

We attached to this document the technical specifications ("data sheets") of the instruments used by Kondoh, Okuma and Newland (1995) in there experiments.

Attachment A

Axoclamp 2A amplifier

The following three pages will present the amplifier **Axoclamp 2A amplifier** specifications.

This is a copy of the manufacturer's web page accessed in June 2016, and available at: `https://www.moleculardevices.com/systems/conventional-patch-clamp/axoclamp-900a-microelectrode-amplifier`.

Axoclamp 900A Amplifier

For two-electrode voltage clamp recordings, whole-cell current-clamp recordings, intracellular sharp electrode recordings, extracellular field potential recordings in ion channel, neuroscience, oocyte and iontophoresis studies

Request Pricing or Quote (/quote-request?pid=224)

Support (http://mdc.custhelp.com/app/ask/)

Axoclamp 900A Microelectrode Amplifier is a complete microelectrode current clamp and voltage clamp amplifier, useful for a wide range of intracellular microelectrode recording techniques.

Overview Applications Software Specs & Configs Resources Order Citations

General Specifications

General Specifications	
Dimensions (in.)	4.3 (H) x 19 (W) x 14.3 (D)
Dimensions (cm)	10.9 (H) x 48.3 (W) x 36.3 (D)
Weight	9.5 lbs. (4.3 kg)
Headstage (in.)	0.75 (H) x 0.70 (W) x 2.25 (D)
Headstage (cm)	1.9 (H) x 1.8 (W) x 5.7 (D)
Rack use	Bayonet feet
Power	100-240 VAC 50-60 Hz, 30 W max
Safety	CE marking (Conformité Européenne)

Detail Specifications

Downloadable PDF Datasheet (http://go.moleculardevices.com/l/83942/2015-06-17/nfh/83942/4366/AxoClamp_900A_Datasheet__rev_C.pdf)

Configurations

Axoclamp 900A Headstages

Maximum Current*						
		I-Clamp	HVIC	TEVC	dSEVC	DCC
Headstage	Ro	(Ch1 &2)	(Ch2)	(Ch2)	(Ch1)	(Ch1)
HS-9Ax0.1U	100M	0.12µA	1.8µA	1.8µA	0.036µA	0.036µA
HS-9Ax1U	10M	1.20µA	18.0µA	18.0µA	0.360µA	0.360µA
HS-9Ax10U	1M	12.00µA	180.0µA	180.0µA	3.600µA	3.600µA

*Maximum current specifications assume negligible electrode resistance.

Axoclamp 900A Headstages

Description	Details	Part Number
Axoclamp 900A Headstage HS-9A X0.1U	x0.1 headstage	1-2950-0359
Axoclamp 900A Headstage HS-9A X1U	x1 headstage	1-2950-0360
Axoclamp 900A Headstage HS-9A X10U	x10 headstage	1-2950-0361
Axoclamp 900A Headstage VG-9A X10U	x10 virtual ground headstage	1-2950-0362
Axoclamp 900A Headstage VG-9A X100U	x100 virtual ground headstage	1-2950-0363

SoftPanel Interface

To offer a more conventional interface to amplifier control, the optional SoftPanel was designed as a hardware extension to replicate all essential amplifier functions by acting as a hardware extension to the Axoclamp and MultiClamp Commander Software. The SoftPanel controller communicates with the computer via an easy-to-set up USB 2.0 connection.

Using the SoftPanel knobs replicate continuous mouse controls ("gliders"), while buttons replicate single-click mouse controls without negating the many benefits afforded by computer control of the amplifier.

(https://www.moleculardevices.com/sites/default/files/product-images/axon-product-images/Axoclamp%20900A%20%20frontal.png)

Axon Conventional Patch Clamp (/Systems/Axon-Conventional-Patch-Clamp)

Axopatch 200B (/systems/axon-conventional-patch-clamp/axopatch-200b-amplifier)

MultiClamp 700B (/systems/conventional-patch-clamp/multiclamp-700b-microelectrode-amplifier)

Axoclamp 900A (/systems/conventional-patch-clamp/axoclamp-900a-microelectrode-amplifier)

Digidata 1550B (/systems/axon-conventional-patch-clamp/digidata-1550b-plus-humsilencer)

pCLAMP 10 Software (/systems/conventional-patch-clamp/pclamp-10-software)

Axoporator 800A (/systems/conventional-patch-clamp/axoporator-800a)

Accessories (/systems/conventional-patch-clamp/axon-accessories)

Related Content

Axoclamp 900A Amplifier Datasheet (http://go.moleculardevices.com/l/83942/2015-06-17/nfh/83942/4366/AxoClamp_900A_Datasheet__rev_C.pdf)

Follow Us:

(http://www.linkedin.com/company/molecular-devices)

(https://www.facebook.com/MolecularDevices) (https://twitter.com/moldev)

(http://www.youtube.com/user/MolecularDevicesInc)

(https://plus.google.com/+moleculardevices/posts)

Attachment B

CG-742, NF Circuit Design Block

The following two pages will present the oscillator **CG-742** specifications.

This is a copy of the manufacturer's web page accessed in June 2016, and available at: `http://www.nfcorp.co.jp/english/pro/fm/osc/index.html`.

Filter
Amplifier
Oscillator
Phase Detector
Customaized Products

Oscillator

Resister Tunable Oscillator

CG series

CG-102R1

CG-402R1

The CG series is a resister tunable sine-wave oscillator which can be set the oscillation frequency with externally connected resistors.

Model	Frequency range	Frequency setting	Output voltage	Distortion factor	Package
CG-102R1	20Hz to 20kHz	2 externally connected resistors	2.5Vrms (0.5V to 20Vp-p is possible.)	0.005% max. (70Hz to 10kHz)	24 pins Dual-in-line package
CG-102R2	1kHz to 100kHz			0.005% max. (2kHz to 50kHz)	
CG-202R3	100kHz to 1MHz		2.5Vrms (1.6V to 5Vrms is possible.)	-50dB typ. (1MHz)	
CG-302R1	20Hz to 20kHz		2.5Vrms (0.5V to 20Vp-p is possible.)	0.005% max. (70Hz to 10kHz)	20 pins Single-in-line package
CG-302R2	1kHz to 100kHz			0.005% max. (2kHz to 50kHz)	
CG-402R1	20Hz to 20kHz		2.5Vrms (±2V to ±10Vrms is possible.)	0.1% max. (200Hz to 100kHz)	12 pins Single-in-line package
CG-402R2	1kHz to 100kHz				

Supply voltage : ±15V

CG-742N Random Binary Generator

Random binary generator is oscillator which can be output binary signal of random timing. It is possible to make white noise combination with lowpass filter.

Noise generator	Pseudo random M series
Basic oscillation frequency	Depends on an externally connected resistor or external clock of TTL level Gain Amplifier
Basic oscillation frequency range	0.5MHz to 5MHz (externally connected resistor) 5MHz max. (external clock)
Output	TTL level or ±5V (no load)
Supply voltage	±15V
Dimensions	54.4 x 33.7 x 9.4 (mm), 40 pins Dual-in-line packager

OP-102 OSCILLATOR ADAPTER

OP-102 can be combined with DT-212D series to enable implementation of sinewave oscillator with the

frequency set by a 3-digit BCD input.

Oscillation frequency range	1Hz to 100kHz Eternally connected components are necessary in 100Hz or lower

◀ Back Top of this page ▲

Attachment C

SR-4BL, NF Circuit Design Block

The following two pages will present the filter **SR-4BL** specifications.

This is a copy of the manufacturer's web page accessed in June 2016, and available at: `http://www.nfcorp.co.jp/english/pro/fm/fil/res/sr/index.html`.

Filter
- Resistor Tunable Filter
- Voltage Tunable Filter
- Programmable Filter
- Fixed Frequency Filter
- Filter for specified application

Amplifier

Oscillator

Phase Detector

Customaized Products

Filter

Resistor Tunable Filter — SR/SRA/SV series

SR-2BLH

SRA-4BL

SR / SRA series

SR Series : For general purpose
SRA Series : Low power Consumtion

Model	Characteristics	Rolloff	Cut-off (center) frequency range			Frequency setting
			Type 1	Type 2	Type 3	
SR-4BL	LPF, 4-pole Butterworth	24dB/oct	40Hz to 1.6kHz	400Hz to 20kHz	5Hz to 100kHz	4 externally connected resistors
SRA-4BL				-	-	
SR-4FL	LPF, 4-pole Elliptic	42dB/oct, equivalent	40Hz to 1.6kHz	400Hz to 20kHz	5Hz to 100kHz	
SRA-4FL				-	-	
SR-4BH	LPF, 4-pole Butterworth	24dB/oct	40Hz to 1.6kHz	400Hz to 5kHz	-	
SRA-4BH				-	-	
SR-4FH	HPF, 4-pole Butterworth	42dB/oct, equivalent	40Hz to 1.6kHz	400Hz to 5kHz	-	
SRA-4FH				-	-	
SR-2BLH	LPF, 2-pole Butterworth	12dB/oct	40Hz to 1.6kHz	400Hz to 20kHz	5Hz to 100kHz	2 externally connected resistors
SR-1BP	BPF, 1-pole pair, Q=5 to 50	6dB/oct BW	40Hz to 1.6kHz	400Hz to 10kHz	-	
SR-2BP	BPF, 2-pole pair, Q=5	12dB/oct BW	40Hz to 1.6kHz	400Hz to 10kHz	-	4 externally connected resistors
SRA-2BP				-	-	
SR-2BE	BEF, 2-pole pair, Q=5	Max. attenua-tion 60dB	40Hz to 1.6kHz	400Hz to 10kHz	-	

Supply voltage : ±15V
Dimensions : 51.5 x 14 (mm), 20 pins, Single-in-line package (SIP)
* Can be installed in Multichannel SR Filter 3315

SV-4BL

SV-4FL

SV Series

SV Series : 5,5V or 3,3V of single supply voltage

Model	Characteristics	Rolloff	Cut-off (center) frequency range		Supply voltage	Frequency setting
			Type 1	Type 2		
SV-4BL	LPF, 4-pole Butterworth	24dB/oct	10Hz to 10kHz	100Hz to 100kHz	5V or 3.3V, single supply voltage	4 externally connected resistors
SV-4FL	LPF,4-pole Elliptic	42dB/oct equivalentt				

◀ Back

Top of this page ▲

Attachment **D**

RD-101 T, TEAC, Japan

The following two pages will present the data recorder **RD-101 T** specifications.

This is a copy of the manufacturer's web page accessed in June 2016, and available at: `http://www.atecorp.com/products/teac/rd-101t.aspx`.

Teac RD 101T DAT PCM Data Recorder

Request Quote
Print Page
Email Page
Like
Specifications

Features:

High-quality data (accuracy)

- The quadruple oversampling digital filter is used as the output stagein the multiplex PCM recording method. The signal-to-noise ratio is 70 dB. The frequency characteristic flatness is +0.5 dB, -1 dB. The phase difference between channels is 5° (fmax).

Multi-channels and wide band

- The RD-101T uses a 2-channel/4-channel switching system. The band for 2-channel recording is 20 kHz and the band for 4-channel recording is 10 kHz.

Small and compact

- The data recorder is approximately 306 mm wide x 100 mm high x 307 mm deep, and weighs approximately seven kilograms. The data recorder is therefore very portable.

Long recording time

- When a 120 tape (approximately 60 m) is used, data can be recorded continuously for two hours.

Three power supplies

- Operates on either AC input of 90-130 (180-250) volts, DC input of 11-30 volts, which are provided normally, and an optional rechargeable battery unit. The battery unit can be incorporated by mounting it on the data recorder. Since the battery charge function is built into the data recorder and protection for battery over-discharging is provided, the RD-101T can be used both indoors and outdoors.

Easy operation (condition setting is unnecessary)

- The input range is fixed to eliminate the need for complicated range setting. The purpose of this function is to approach the absolute value recording by making the input and output voltages equal:

Memo sound channel

- In addition to the data channels, a channel used only for voice recording and reproduction is provided. Since the microphone built into the data recorder is provided normally for recording, environmental sounds can always be recorded during measurement.

Time code recording channel

- In addition to the data channels, a channel used only for recording and reproduction of time codes is built in. The year, month, day, hours, minutes, and seconds of the built-in clock with perpetual calendar are automatically recorded. Since the time code is always automatically recorded, it can be used to confirm the recording time of measurement

data on the display.

Data number (ID number) recording channel

- In addition to the data channels, a channel used only for recording and reproduction of ID numbers is built in. The ID number of the recorded data is automatically recorded. The ID number is incremented by one each time recording starts or the EVENT button is pressed.

High-speed search

- The recorded ID number can be searched for at high speed during reproduction. The search is performed both in the forward and reverse directions. When the target ID number is found, the target data is reproduced from the beginning.
  Pressing the PAUSE button during search causes the tape to pause at the beginning of the data when the search ends.

Bar meter monitor

- All channels can be monitored at one time with the 6-point display bar meters. In this case, the memo sound channel can also be monitored. The signal level can be monitored both during recording and reproduction.

Related Products

Honeywell 101E Chart Recorder

View Product

Kyowa RTP650A Data Recorder

View Product

Sony PC116 Digital Instrumentation Data Recorder

View Product

Sony PC216A 16 Channel Digital Data Recorder

View Product

Sony SIR-1000W-STB-10 Digital Data Recorder

View Product

Teac CR524M Communication Recorder

View Product